

# Measurement Report: Investigation on the sources and formation processes of dicarboxylic acids and related species in urban aerosols before and during the COVID-19 lockdown in Jinan, East China

Jingjing Meng<sup>1,2</sup>, Yachen Wang<sup>1</sup>, Yuanyuan Li<sup>1</sup>, Tonglin Huang<sup>1</sup>, Zhifei Wang<sup>3</sup>, Yiqiu, Wang<sup>4</sup>, Min Chen<sup>1</sup>, Zhanfang Hou<sup>1</sup>, Houhua Zhou<sup>5</sup>, Keding Lu<sup>5</sup>, Kimitaka Kawamura<sup>6</sup>, Pingqing Fu<sup>2</sup>

<sup>1</sup> School of Geography and Environment, Liaocheng University, Liaocheng 252000, China

<sup>2</sup> Institute of Surface-Earth System Science, School of Earth System Science, Tianjin University, Tianjin 300072, China

<sup>3</sup> Jinan Environmental Monitoring Center of Shandong Province, Jinan 250101, China

<sup>4</sup> Liaocheng Environmental Information and Monitoring Center, Liaocheng, 252000, China

<sup>5</sup> State Key Joint Laboratory of Environmental Simulation and Pollution Control, College of Environmental Sciences and Engineering, Peking University, Beijing 100871, China

<sup>6</sup> Chubu Institute for Advanced Studies, Chubu University, Kasugai 487-8501, Japan

*Correspondence to:* Pingqing Fu (fupingqing@tju.edu.cn)

**Abstract.** Dicarboxylic acid (Diacid) homologues are essential indicators of secondary organic aerosols (SOA) that exert considerable influence on climate changes and atmospheric chemistry. However, their sources and formation processes are poorly understood, leading to uncertainty in predicting the climate effect of SOA. A substantial drop in anthropogenic emissions during the COVID-19 lockdown (LCD) provides a “controlled experiment” to explore the effects of LCD measures and meteorological conditions on SOA. Here we investigated the difference in molecular distributions and stable carbon isotopic compositions ( $\delta^{13}\text{C}$ ) of diacid homologues in  $\text{PM}_{2.5}$  before and during the LCD. We found that the concentration and contribution of diacid homologues during the LCD were higher than before the LCD, indicating that the enhanced secondary oxidation could offset the reduction of anthropogenic emissions during the LCD. Higher oxalic acid ( $\text{C}_2$ )/diacids ratio and more positive  $\delta^{13}\text{C}$  values of major diacids during the LCD suggested more aged organic aerosols. The enhanced  $\text{C}_2$  and related species during the LCD were mainly derived from the promoted gaseous photochemical oxidation by the higher oxidants and stronger solar radiation. However,  $\text{C}_2$  and related species before the LCD were dominantly derived from the aqueous oxidation of  $\alpha$ -dicarbonyls depending on relative humidity and liquid water content. The increased  $\delta^{13}\text{C}$  values of  $\text{C}_2$  and other major diacids along with the high ratios of  $\text{C}_2$ /glyoxal,  $\text{C}_2$ /methylglyoxal, and  $\text{C}_2$ /diacids confirmed an isotopic fractionation effect during the oxidation process of precursors. Our results indicate that atmospheric pollution treatment depends on a balanced strategy and coordinated effort to control multiple pollutants.

# 1 Introduction

Water-soluble organic compounds (WSOC), constituting a great proportion of atmospheric fine particles, have attracted growing attention for the adverse effects on haze formation and global climate change (Lv et al., 2022; Wang et al., 2016). Dicarboxylic acids (diacids) and their organic precursors such as oxocarboxylic acids (oxoacids) and  $\alpha$ -dicarbonyls are ubiquitous in the atmosphere, accounting for 14% of WSOC in particulate matter of urban regions (Ho et al., 2007; Kawamura and Bikkina, 2016), and can be up to 52% in marine regions (Bikkina et al., 2015). Due to the high solubility and hygroscopicity, diacid homologues can not only modify the hygroscopic growth of aerosols but also improve the cloud condensation nuclei (CCN) activation, thus they exert an important effect on radiative forcing of aerosols via scattering the solar radiation and cloud formation (Ding et al., 2021; Wang et al., 2015).

Diacids and related compounds can be emitted directly from biogenic sources (Rinaldi et al., 2011), vehicle exhausts (Kawamura and Kaplan, 1987), and combustions of biomass and fossil fuels (Cao et al., 2017; Narukawa et al., 1999), while their relative contribution to total aerosol mass is negligible (Shen et al., 2022; Wang et al., 2020a). A growing body of evidence from modeling studies, chamber experiments, and field measurements inside and outside clouds have highlighted that most of these water-soluble organic acids are predominantly generated from the photochemical oxidation of volatile organic compounds (VOCs) followed by partitioning into the aqueous phase in wet aerosols, fog, and cloud droplets (Carlton et al., 2007; Chen et al., 2022; Ervens et al., 2004, 2011; Fu et al., 2008; Lim et al., 2013; Shen et al., 2022; Wang et al., 2010). Therefore, diacid homologues have been regarded as essential indicators of SOA in the atmosphere, which have been increasingly used to trace the aging processes and assess the oxidative capacity of the atmosphere (Enami et al., 2015; Zhao et al., 2020).

As the most abundant diacid with the lowest molecular weight, oxalic acid ( $C_2$ ) is an important end product of numerous formation pathways in aerosols; thus its formation mechanism has attracted great attention in the last decade. The strong correlation of  $C_2$  with  $SO_4^{2-}$  at different observation sites suggests that both species shared a common production pathway (i.e., in-cloud processing) (Ding et al., 2021; Jung et al., 2010; Shen et al., 2023; Yu et al., 2005). A modeling study by Warneck (2003) revealed that the in-cloud formation pathway of  $C_2$  from the oxidation of olefins with  $OH \cdot$  radicals is crucially mediated by glyoxylic acid ( $\omega C_2$ ). A field study in the marine atmosphere by Crahan (2004) further supported such a formation mechanism of  $C_2$ . However, Carlton et al. (2007) conducted chamber experiments and found that glyoxal (Gly) is oxidized by  $OH \cdot$  radicals in the aqueous phase to produce larger multifunctional compounds (not  $\omega C_2$ ) and ultimately degraded into  $C_2$ . This formation route of  $C_2$  is different from the in-cloud processing. Furthermore, the  $C_2$  formation via the  $\omega C_2$  pathway only accounts for less than 1% (Carlton et al., 2007). Perri et al. (2009) first confirmed that the oxidation of glycolaldehyde with  $OH \cdot$  radicals can not only produce  $C_2$ , glycolic acid, and  $\omega C_2$ , but also form oligomer, malonic acid ( $C_3$ ), and succinic acid ( $C_4$ ). Many studies have demonstrated that  $C_2$  is also derived from the photochemical breakdown/decomposition of longer-chain diacids such as  $C_3$  and  $C_4$  (Kawamura and Usukura, 1993; Meng et al., 2021; Yu et al., 2021), but this process has been considered less important than the  $C_2$  formation through the aqueous  $OH \cdot$  radical oxidation (Carlton et al., 2007; Xu et al., 2022). Yu et al. (2019) reported that aqueous oxidation exerts a dominant effect on diacids and related compounds despite the increased contribution of photochemical oxidation in the gaseous phase during haze events in Beijing using multiple linear regression. A recent study by Xu et al. (2022) pointed out that a large portion of  $C_2$  was derived from the aqueous process of organic precursors emitted from fossil fuel combustions. Laboratory simulation has demonstrated that  $C_2$  can be oxidized by  $O_3$  (Gligorovski et al., 2010), while field measurements have demonstrated that formation pathways influenced by  $O_3$  are involved in the formation of  $C_2$  (Meng et al., 2021; Mochizuki et al., 2017). The formation mechanism and influencing factors as well as the contribution of aqueous oxidation and gaseous photochemical oxidation are still not well understood. Therefore, further investigations on  $C_2$  and related compounds are necessary to provide a knowledge base for a better understanding of SOA and improve the accuracy of the aerosol model.

To curb the transmission of the novel coronavirus disease 2019 (hereafter referred to as COVID-19) in human society, a strict lockdown (LCD) measure was first implemented by the Chinese government at the end of January 2020 (Le et al., 2020). These dramatic restrictions resulted in a sharp drop-off in air pollutants (Li et al., 2021a; Meng et al., 2021), for instance, the average concentrations of five parameters including CO, NO<sub>2</sub>, SO<sub>2</sub>, PM<sub>2.5</sub>, and PM<sub>10</sub> decreased by 4.6–24.7% in 44 cities of China because of the travel restrictions during the LCD (Bao and Zhang, 2020). Unexpectedly, a few haze episodes still occurred in China during the LCD. Online observations, model simulations, and satellite measurements have pointed out that the appearance of haze events during the LCD was mainly caused by the unfavorable meteorological conditions, continuous emissions of SO<sub>2</sub>, NO<sub>x</sub>, and VOCs from power plants and petrochemical refineries, and enhanced SOA formation (Huang et al., 2020; Li et al., 2020; Wang et al., 2020b; Shi et al., 2021; Zhong et al., 2021). These studies focused on the effect of the LCD policies on air quality and haze formation, for example, Le et al. (2020) and Huang et al. (2020) pointed out that the reduction of NO<sub>x</sub> emissions leads to enhanced ozone concentration, further improved the atmospheric oxidizing capacity and promoted the formation of secondary aerosol during the LCD. However, little is known about the impact of LCD measures on the molecular distributions, aging processes, and the formation mechanisms of SOA from field observations.

In order to understand the effect of the reduced anthropogenic emissions during the LCD and different meteorological parameters on the evolutionary process of homologous diacids and to investigate the relative contribution of aqueous oxidation versus gas-phase photochemical oxidation to total diacid homologues, fine aerosol samples in urban the city of Jinan, East China on a day/night basis before and during the LCD were collected. In this study, we first compare the differences in the molecular distributions, stable carbon isotopic compositions, and formation processes of C<sub>2</sub> and the related SOA before and during the LCD. Then, we investigate the effect of meteorological parameters (e.g., RH, temperature, and solar radiation) and aerosol aqueous properties (e.g., liquid water content (LWC) of aerosol and particle acidity (pH<sub>is</sub>)) on their formation processes in the urban atmosphere.

## 2 Experimental methods

### 2.1 Aerosol sampling

Fine aerosol (PM<sub>2.5</sub>) sampling was conducted on the rooftop of a six-story building (36.67°N, 117.06°E, approximately 20 m above ground) that was about 40 m away from the Jinan Environment Monitoring Center (one of the State Controlling Air Sampling Sites in Jinan). The sampling site is in the center of the city of Jinan, which is located in the midwestern part of Shandong Province, China (Fig. S1). The sampling site lies in a typical urban setting surrounded by heavy traffic roads, residential areas, and commercial centers. PM<sub>2.5</sub> samples were collected using prebaked (450 °C, 8 h) quartz fiber filters (8 in. × 10 in.) from 6 January to 17 February 2020. The provincial government first performed the preventive LCD starting on 24 January 2020; thus the whole sampling period was divided into two periods: (1) before the LCD from 6 to 23 January, (2) during the LCD from 31 January to 17 February. Each sample lasted for 12 h on a day/night basis using a high-volume air sampler (TISCH, USA) at an airflow rate of 1.01 m<sup>3</sup> min<sup>-1</sup>. The daytime samples were collected from 8:00 to 20:00, while nighttime samples were collected from 20:00 to 8:00 the next day. The field blank was sampled to check whether or not the aerosol samples had been polluted during the operation process, including the placing and collecting processes of the filter, which took about a few minutes. The operating procedure of collecting field blank samples for 10 min in this study is conventional and scientifically sound and was also confirmed in other studies (Qi et al., 2022; Yi et al., 2021). Therefore, field blank samples were also collected by mounting the blank filter onto the sampler for 10 min without turning on the sampler before, during, and after the sampling campaign, respectively.

A total of 72 PM<sub>2.5</sub> samples (36 for daytime and 36 for nighttime) and 6 field blank samples were collected in the whole sampling period. After the collection, each filter was sealed in an aluminum foil bag and stored in a freezer (–20 °C) for

about 16 months prior to analysis. The concentrations of PM<sub>2.5</sub>, PM<sub>10</sub>, CO, SO<sub>2</sub>, NO<sub>2</sub>, and O<sub>3</sub>, as well as meteorological parameters such as wind direction/speed, RH, temperature, and solar radiation were retrieved from the monitoring station in the Jinan Environment Monitoring Center (<https://www.aqistudy.cn/>). The detailed information on quality assurance/quality control (QA/QC) of online data was described in Text S4. The inlet height of the air quality monitoring station was approximately 20 m above the ground level.

## 2.2 Chemical Analysis

### 2.2.1 Determination of diacids and related compounds as well as levoglucosan

The quantitative method for analyzing diacids, oxoacids, and  $\alpha$ -dicarbonyls in PM<sub>2.5</sub> has been described previously (Fu et al., 2013; Meng et al., 2020). Briefly, a quarter of the filter was extracted with 5 mL pure Milli-Q water under ultrasonication three times. The water extracts were concentrated to near dryness and then reacted with 14% BF<sub>3</sub>/*n*-butanol at 100 °C for 1 hour. During this process, the carboxyl functional group was derivatized to butyl ester, and the aldehyde and keto groups were derivatized to dibutoxy acetal. After derivatization, *n*-hexane was added and washed with pure water three times. Finally, the hexane layer was determined by a gas chromatography-mass spectrometry (GC-MS) and quantitatively analyzed using a GC (Agilent 6980) coupled with an HP-5 column (0.2mm × 25m, 0.5 μm film thickness) and a flame ionization detector (FID). GC-MS was performed on a Hewlett-Packard model Agilent 7890A GC coupled to a Hewlett-Packard model Agilent 5975C mass selective detector (MSD). GC separation was equipped with a split/splitless injector and a fused silica capillary column (DB-5MS, 30 m × 0.25 mm i.d., 0.25 μm film thickness). The GC oven temperature was programmed from 50°C for 2 min to 120°C at a rate of 15°C min<sup>-1</sup>, and then to 300°C at a rate of 5°C min<sup>-1</sup> with a final hold at 300°C for 16 min. The mass spectrometer was operated on the electron impact (IE) mode at 70 eV and scanned from 50 to 650 Da. The same analytical method as described above was also applied for field blank filters. As described in previous studies, the recoveries of C<sub>2</sub> ranged from 70% to 83% and other target compounds were better than 80% (Ding et al., 2021; Kawamura et al., 2013; Kawamura and Yasui, 2005; Meng et al., 2020; Zhao et al., 2020). Recoveries of the target compounds in this study were 80% for C<sub>2</sub> and higher than 85% for other organic species. Therefore, the percent recoveries mentioned in this study were good enough for such analysis.

Additionally, another portion of each filter sample was extracted with a mixture of dichloromethane and methanol (2:1, v/v) under ultrasonication. After being derivatized with a 60 μL mixture of N, O-bis-(trimethylsilyl) trifluoroacetamide (BSTFA) and pyridine (5:1, v/v) at 70°C for 3 h, the derivatized extracts were identified for levoglucosan using a GC-MS (Yi et al., 2021). The recovery rate of levoglucosan is higher than 95%. Compared with the ambient samples, the concentration of levoglucosan in the field blank samples was lower than 4%. The data of targeted organic species presented in this study were corrected for both recoveries and field blanks.

### 2.2.2 Stable carbon isotopic composition of diacids and related compounds

The stable carbon isotopic compositions ( $\delta^{13}\text{C}$ ) of major diacids and related compounds were measured using the method reported elsewhere (Kawamura and Watanabe, 2004). Briefly, 2 μL internal standard (*n*-C<sub>13</sub> alkane, -27.24 ‰) was spiked to the ester fraction, and the  $\delta^{13}\text{C}$  values of the derivatized samples relative to Pee Dee Belemnite (PDB) were measured using a GC-isotope ratio MS (GC-IR-MS, Thermo Fisher, Delta V Advantage). GC was installed with an HP manual on-column injector and a capillary column (CIP-Sil 8CB, 60 m × 0.32 mm × 0.25 μm) was used with a column oven temperature programmed from 50 to 120°C at a rate of 30°C min<sup>-1</sup> and then to 300°C at a rate of 6°C min<sup>-1</sup>. Flow rate of carrier gas (He) was maintained at 1.7 mL min<sup>-1</sup>. Each sample was measured twice or three times to check the analytical error of the  $\delta^{13}\text{C}$  values, which were less than 0.2‰. The  $\delta^{13}\text{C}$  values were then calculated for free organic acids using an isotope mass balance equation based on the measured  $\delta^{13}\text{C}$  values of derivatives and the derivatizing agent (BF<sub>3</sub>/*n*-butanol), as detailed in Text S1 (Kawamura and Watanabe, 2004).

### 155 2.2.3 Elemental carbon (EC), organic carbon (OC), WSOC, and inorganic ions

EC and OC in the PM<sub>2.5</sub> samples were analyzed using a DRI Model 2015 Carbon Analyzer following the Interagency Monitoring of Protected Visual Environments (IMPROVE) thermal/optical reflectance (TOR) protocol (Chow et al., 2004). As for the measurement of inorganic ions and WSOC, an aliquot of each sample filter was extracted with 30 mL Milli-Q water using an ultrasonic bath three times and then filtered through PTFE filters to remove particles and filter debris. The water extract was then divided into two parts. One part was analyzed for inorganic ions using ion chromatography (Dionex 160 600, USA), and the other part was used to determine WSOC using a Total Carbon Analyzer (TOC-L CPH, Shimadzu, Japan).

### 2.3 Calculation of aerosol liquid water content (LWC), particle in-situ pH (pH<sub>is</sub>), and OH·radicals

As for the calculation of aerosol LWC and pH<sub>is</sub>, the ISORROPIA-II model that treated the Na<sup>+</sup> - NH<sub>4</sub><sup>+</sup> - K<sup>+</sup> - Ca<sup>2+</sup> - Mg<sup>2+</sup> - SO<sub>4</sub><sup>2-</sup> - NO<sub>3</sub><sup>-</sup> - Cl<sup>-</sup> system was applied. The forward mode with a metastable state in the ISORROPIA model was adopted (Fountoukis and Nenes, 2007).

Because of its short lifetime, high reactivity, and low concentration, the concentration of OH·radicals in the atmosphere is difficult to measure. Therefore, we used the TUV model (5.3 version) to calculate the time series of photolysis frequencies of ozone ( $J(O^1D)$ ) before and during the LCD in Jinan and then multiplied it by a factor of  $4 \times 10^{11}$  to estimate the corresponding time series of OH·radical concentration (molecules cm<sup>-3</sup>), based on the approximate linear relationship of OH·radical concentration to  $J(O^1D)$  (Lu et al., 2019).

## 3 Results and Discussion

### 3.1 Meteorological conditions and air pollutants before and during the LCD

Temporal variations in the concentrations of PM<sub>2.5</sub>, PM<sub>10</sub>, gaseous pollutants, major chemical components of PM<sub>2.5</sub>, and meteorological parameters before and during the LCD are summarized in Table 1 and presented in Fig. 1. Both temperature and solar radiation exhibited a continuously increasing trend, whereas RH before the LCD was 1.4 times higher than that during the LCD. Wind speed ( $3.0 \pm 0.7$  m s<sup>-1</sup>) before the LCD was smaller than that ( $3.7 \pm 1.1$  m s<sup>-1</sup>) during the LCD (Table 1), suggesting that air pollution caused by emissions from the local and surrounding regions of Jinan before the LCD was greater than that during the LCD, which was supported by the results of backward trajectory and potential source contribution function (PSCF) analysis (Fig. S1).

The parameters of air quality including PM<sub>2.5</sub>, PM<sub>10</sub>, CO, SO<sub>2</sub>, and NO<sub>2</sub> decreased by 39–62% during the LCD (Table 1, Fig. 1), suggesting that the air quality was better during the LCD because of the substantial reduction of anthropogenic emissions. The haze event is defined as the daily average concentration of PM<sub>2.5</sub> larger than the Grade II of the Chinese National Ambient Air Quality Standard ( $75 \mu\text{g m}^{-3}$ ) (Huang et al., 2014; Li et al., 2021b). Thirteen haze days before the LCD and four haze days during the LCD were observed in Jinan, respectively. Additionally, solar radiation ( $255 \pm 117$  W m<sup>-2</sup>) during the LCD was stronger than that ( $164 \pm 70$  W m<sup>-2</sup>) before the LCD (Table 1). It could be concluded that the atmosphere was clearer during the LCD than before the LCD, albeit the occurrence of several haze days. Being opposite to the other five air-quality parameters, O<sub>3</sub> concentration ( $66 \pm 21 \mu\text{g m}^{-3}$ ) during the LCD increased by 2.3 times compared to that ( $29 \pm 18 \mu\text{g m}^{-3}$ ) before the LCD (Table 1). Wang et al. (2021) demonstrated that O<sub>3</sub> in Chinese megacities during the LCD is primarily produced from the NO<sub>x</sub>-saturated regime. The significant drop of NO<sub>2</sub> during the LCD led to the reduction of NO concentration (Xu et al., 2020), and further weakened the efficient titration effect of O<sub>3</sub> (Levy et al., 2014). Thus, the lower concentration of NO<sub>2</sub> during the LCD could increase O<sub>3</sub> concentration. O<sub>3</sub> exhibited a negative correlation with PM<sub>2.5</sub> mass concentration ( $R^2 = 0.57$ ) during the LCD, suggesting that the enhanced O<sub>3</sub> was also driven by lower PM<sub>2.5</sub> concentration

195 during the LCD because  $PM_{2.5}$  could scavenge the precursors ( $HO_2 \cdot$  and  $NO_x$  radicals) of  $O_3$  (Li et al., 2019) and alleviate the aerosol radiative effect on the photochemical formation of  $O_3$  (Wu et al., 2020). Moreover, the more favorable atmospheric conditions such as the higher temperature and stronger solar radiation during the LCD were beneficial for the generation and accumulation of  $O_3$  (Li et al., 2019). Being consistent with the variation of  $O_3$  concentration, the concentration of  $OH \cdot$  radicals during the LCD ( $1.4 \times 10^7 \text{ cm}^{-3}$ ) was 1.4 times higher than that ( $9.7 \times 10^6 \text{ cm}^{-3}$ ) before the LCD (Table 1), which was also observed in other studies (Gaubert et al., 2021; Kang et al., 2021). The reduced  $NO_x$  during  
200 the LCD could lead to a higher concentration of  $OH \cdot$  radicals because less  $OH \cdot$  radicals could be consumed with  $NO_2$  to produce nitric acid (Gaubert et al., 2021). Additionally, the elevated  $O_3$  concentration during the LCD could result in the enhanced  $OH \cdot$  radicals, as  $OH \cdot$  radicals are mainly derived from  $O_3$  photolysis with water vapor in the atmosphere (Kang et al., 2021).

The decreased concentrations of EC, OC, and WSOC in  $PM_{2.5}$  but the enhanced ratios of OC/EC and WSOC/OC during the LCD (Table 1, Fig. 1) indicated more SOA productions due to the stronger photochemical oxidation during the LCD (Zhong et al., 2021). As a key tracer for biomass burning, levoglucosan showed a positive relationship with OC, EC, and WSOC ( $R^2 \geq 0.45$ ) before the LCD rather than during the LCD ( $R^2 \leq 0.15$ ) (Table S1), suggesting that biomass burning played an important role in carbonaceous species before the LCD rather than during the LCD. Secondary inorganic ions (SIA, the total concentration of  $SO_4^{2-}$ ,  $NO_3^-$ , and  $NH_4^+$ ) were dominant components of  $PM_{2.5}$ , which accounted for the higher percentages (47 ± 8%) in  $PM_{2.5}$  mass during the LCD than that (40 ± 6%) before the LCD, indicating an enhanced formation of secondary aerosols during the LCD. The results of backward trajectory analysis showed that air masses before and during the LCD in Jinan were different (Fig. S1). Thus, the differences in the above chemical species and ratios may be not only because of different emission strengths and types of sources but also due to different air masses between these two periods. The LWC concentration of aerosol is determined by RH and SIA concentration (Meng et al., 2020). Given the higher RH and SIA concentration before the LCD, the LWC concentration ( $35 \pm 33 \mu\text{g m}^{-3}$ ) before the LCD was 3.4 times higher than that ( $10 \pm 10 \mu\text{g m}^{-3}$ ) during the LCD. However,  $pH_{is}$  remained similar before ( $3.2 \pm 3.0$ ) and during the LCD ( $3.5 \pm 3.5$ ) with no significant statistical difference ( $p > 0.05$ , Table S2), indicating an insignificant difference in atmospheric aerosol acidity before and during the LCD.

### 3.2 Comparison of molecular distributions of diacids and related species before and during the LCD

220 A homologous series of diacids ( $C_2$ – $C_{11}$ ), oxoacids, and  $\alpha$ -dicarbonyls identified in  $PM_{2.5}$  samples before and during the LCD are summarized in Table 2. To avoid the effect of atmospheric dilution due to the variations in boundary layer height, we use the ratios of SOA species to EC or CO to explore the secondary production of organic species (Yu et al., 2021). As shown in Fig. 2, the ratio of total concentration of detected organic components (TDOCs) normalized by CO (TDOCs/CO) increased exponentially with the increase of temperature before ( $y = 257.46e^{0.019x}$ ,  $R^2 = 0.56$ , Fig. 5a) and during ( $y = 301.49e^{0.067x}$ ,  $R^2 = 0.58$ , Fig. 5c) the LCD, which was consistent with the Arrhenius Law, confirming that TDCOCs in this study were primarily derived from secondary formation and the contribution of primary emissions was insignificant. TDOCs are considered the stable products of secondary oxidation for a number of hydrocarbons (Martinelango et al., 2007). The loss of diacids (e.g.,  $C_2$ ) through the photolysis of iron oxalate complexes is a dominant sink from field observations and model studies (Cheng et al., 2017; Pavuluri and Kawamura, 2012; Weller et al., 2014; Zhou et al., 2015), while these species are  
230 more stable in the absence of Fe (Kunwar et al., 2019). Previous studies have pointed out that diacids and related compounds presented a strong correlation with temperature, emphasizing the significance of the secondary formation of those compounds with the increase in temperature (Kawamura and Bikkina, 2016; Kawamura and Yasui, 2005; Meng et al., 2014, 2018). Therefore, the loss of diacids and related compounds may be negligible when temperature increases. Additionally, the exponent(0.067) of the regression trend line during the LCD was 3.5 times higher ( $p < 0.05$ ) than that (0.019) before the  
235 LCD, indicating that the oxidation rate during the LCD was larger. Different secondary formation rates of TDOCs between

these two observation periods were possibly due to different meteorological factors (e.g., temperature, solar radiation, and RH), oxidants (e.g., O<sub>3</sub> and OH· radical), emission strengths and types of organic precursors, physicochemical properties of aerosols (e.g., pH<sub>is</sub> and LWC), and other influencing factors.

To verify if the concentrations of target compounds and major ratios were of significant difference, statistic tests were performed for PM<sub>2.5</sub> samples before and during the LCD (Table S2 and Table S3). As shown in Table S2, the concentrations of organic species (except for  $\alpha$ -dicarbonyls) and major ratios in PM<sub>2.5</sub> before and during the LCD presented *p* values less than 0.05, indicating that the abundances and compositions of the major species before and during the LCD were statistically different. TDOCs exhibited an upward trend from  $437 \pm 117 \text{ ng m}^{-3}$  ( $246 - 833 \text{ ng m}^{-3}$ ) before the LCD to  $486 \pm 144 \text{ ng m}^{-3}$  ( $179-825 \text{ ng m}^{-3}$ ) during the LCD (Table 2). The concentrations of diacids and oxoacids during the LCD increased by a factor of 1.1 and 2.1, respectively, while  $\alpha$ -dicarbonyls during the LCD were almost the same as before the LCD. The concentrations of diacids and TDOCs reported in this study were significantly lower than those in Xi'an (Cheng et al., 2013), Chengdu (Li et al., 2015), Tianjin (Devineni et al., 2023; Zhao et al., 2023), Liaocheng (Meng et al., 2020), 14 Chinese cities, and other Asian megacities such as Padori, Daejeon (Zhao et al., 2023), Ulaanbaatar (Jung et al., 2010), Chennai (Pavuluri et al., 2010), and Tokyo (Kawamura and Yasui, 2005), but similar to those in Beijing (Zhao et al., 2018) and Guangzhou (Ho et al., 2011) during the wintertime (Table S4).

The daytime concentration of diacids before the LCD was 17% lower than that at night, which was opposite to the diurnal variation of diacids concentration during the LCD (Fig. 3a). As the predominant species throughout the whole observation period, C<sub>2</sub> concentration increased from  $181 \pm 47 \text{ ng m}^{-3}$  before the LCD to  $239 \pm 108 \text{ ng m}^{-3}$  during the LCD (Table 2), despite of the significant decrease in the primary pollutants from anthropogenic emissions during the LCD. C<sub>2</sub> is an end product derived from the photochemical decomposition of longer-chain diacids or secondary oxidation of  $\alpha$ -dicarbonyls and oxoacids, thus the ratios of C<sub>2</sub>/diacids and C<sub>2</sub>/TDOCs can be considered essential tracers of aerosol aging (Wang et al., 2012; Zhao et al., 2020). Both ratios of C<sub>2</sub>/diacids and C<sub>2</sub>/TDOCs during the LCD were higher than those before the LCD (Fig. 3b), reflecting the presence of more aged organic aerosols during the LCD, which will be given more evidence in Section 3.5. Therefore, the concentration of C<sub>2</sub> as well as its relative abundance in total diacids and TDOCs were higher during the LCD than before the LCD, mainly due to the accelerated formation of C<sub>2</sub> during the LCD, which could offset the drop of organic precursors from anthropogenic emissions (Huang et al., 2020). Moreover, the daytime concentration of C<sub>2</sub> and the ratios of C<sub>2</sub>/TDOCs and C<sub>2</sub>/diacids were lower than those at night before the LCD but the opposite trends were found during the LCD, being consistent with the diurnal changes of total diacids before and during the LCD (Fig. 3). The second most abundant diacid was C<sub>4</sub>, followed by C<sub>3</sub> and azelaic acid (C<sub>9</sub>) before the LCD, while the second dominant diacid during the LCD was C<sub>3</sub>, followed by C<sub>4</sub> and phthalic acid (Ph) (Table 2). Our results suggest that these species had different sources and underwent different formation processes because of different concentration levels of organic precursors and meteorological conditions before and during the LCD.

Both ratios of C<sub>2</sub>/C<sub>4</sub> and C<sub>3</sub>/C<sub>4</sub> have been used as indicators of the photochemical aging of diacids, because the photochemical degradation of C<sub>4</sub> can lead to C<sub>3</sub>, and C<sub>3</sub> can be photochemically oxidized into C<sub>2</sub> via intermediates (e.g., ketomalonic (kC<sub>3</sub>) and hydroxymalonic acids) (Kawamura and Bikkina, 2016; Wang et al., 2010). Both C<sub>2</sub>/C<sub>4</sub> ( $8.4 \pm 3.4$ ) and C<sub>3</sub>/C<sub>4</sub> ( $1.6 \pm 0.4$ ) ratios during the LCD were higher than those ( $3.9 \pm 1.5$ ,  $0.3 \pm 0.1$ ) before the LCD (Fig. 3b), indicating the stronger photochemical transformation of organic aerosols during the LCD. The C<sub>3</sub>/C<sub>4</sub> ratio before the LCD was lower than that in other Asian megacities such as 14 Chinese cities (Ho et al., 2007), Beijing (Zhao et al., 2018), Daejeon (Devineni et al., 2023), and Chennai (Pavuluri et al., 2010), but comparable to that in Tianjin where biomass burning, biogenic sources, and their aging contributed significantly to diacids and related compounds (Devineni et al., 2023) (Table S4). However, the C<sub>3</sub>/C<sub>4</sub> ratio during the LCD was much higher than that in other Asian megacities (Table S4), again implying the significantly enhanced photochemical oxidation during the LCD. Previous studies have demonstrated that the C<sub>3</sub>/C<sub>4</sub> ratio presented a strong correlation with temperature when the contribution of local sources predominates over long-distance transport

(Kawamura and Usukura, 1993; Pavuluri et al., 2010a; Wang et al., 2020). In this study, the  $C_3/C_4$  ratio was correlated strongly with temperature before the LCD ( $R^2 = 0.54$ , Fig. 4a), indicating that diacids before the LCD were largely influenced by local sources. However, the  $C_3/C_4$  ratio was correlated moderately with temperature ( $R^2 = 0.33$ , Fig. 4b) during the LCD, suggesting that the contribution of local sources was equal to that of long-range transport to diacids during the LCD. These results were consistent with the results of backward trajectory and PSCF analysis (Fig. S1). The higher ratios of  $C_2/C_4$  and  $C_3/C_4$  during the LCD may be due to the local photooxidation and aging effects of long-distance transport.

Azelaic acid ( $C_9$ ) is primarily derived from the secondary oxidation of unsaturated fatty acids (e.g., oleic acid) with a double bond at the C-9 position (Kawamura and Usukura, 1993), which is abundant in the fresh and aged aerosols emitted from biomass burning (Shen et al., 2022). It is noteworthy that the  $C_9$  concentration ( $12 \pm 4.0$ ) before the LCD was 2.0 times higher than that ( $5.9 \pm 4.8$ ) during the LCD (Table 2), consistent with the variation of levoglucosan concentration (Table 1).  $C_9$  showed a more robust relationship with levoglucosan before the LCD ( $R^2 = 0.74$ ) than that ( $R^2 = 0.06$ ) during the LCD (Table S1), suggesting that biomass burning was an essential contributor to  $C_9$  before the LCD rather than during the LCD. Ph is primarily derived from the photochemical degradation of aromatic hydrocarbons (e.g., naphthalene) emitted from anthropogenic sources (Kawamura and Usukura, 1993). Although Ph was the most abundant diacid except for  $C_2 - C_4$  during the LCD, its concentration ( $8.8 \pm 6.1 \text{ ng m}^{-3}$ ) and relative abundance ( $2.3 \pm 2.2\%$ ) in total diacids during the LCD were lower than those ( $11.0 \pm 6.1 \text{ ng m}^{-3}$ ,  $3.2 \pm 1.5\%$ ) before the LCD (Table 2, Fig. 3), suggesting the remarkable drop of anthropogenic emissions during the LCD.

As the important intermediate compounds of mono-carboxylic acids, oxoacids can ultimately generate diacids through aqueous oxidation (Carlton et al., 2007; Ervens et al., 2004). The diurnal variations of oxoacids presented similar patterns with diacids in each period (Fig. 3a). Moreover, oxoacids were correlated well with total diacids in each period, respectively ( $R^2 > 0.5$ , Fig. 2), indicating that oxoacids are the important intermediate species of diacids. The molecular distributions of oxoacids were characterized by the predominance of  $\omega C_2$  and pyruvic acid (Pyr) in each period. Previous studies have demonstrated that  $C_2$  in urban aerosols is mainly generated from  $\omega C_2$  via aqueous oxidation (Cheng et al., 2015; Zhao et al., 2018). Therefore,  $C_2$  was positively correlated with  $\omega C_2$  before and during the LCD, respectively ( $R^2 > 0.5$ , Fig. 4).

As the two smallest molecular weight  $\alpha$ -dicarbonyls in the aerosols, glyoxal (Gly) and methylglyoxal (mGly) originated from the photochemical oxidation of volatile organic compounds such as aromatics, isoprene, and monoterpenes in the gaseous phase, which are then partitioned into the aqueous phase of aerosols, and ultimately are oxidized to relatively lower volatility organic acids (e.g.,  $\omega C_2$ , Pyr, and  $C_2$ ) (Carlton et al., 2007; Fu et al., 2008). Although the anthropogenic source emissions of  $\alpha$ -dicarbonyls decreased dramatically during the LCD, the higher temperature and  $O_3$  concentration during the LCD provided a favorable condition for  $\alpha$ -dicarbonyls productions via secondary oxidation, which could offset the drop of primary emissions. Therefore, the concentration ( $24.7 \pm 10.0 \text{ ng m}^{-3}$ ) of  $\alpha$ -dicarbonyls during the LCD was about equal to that ( $25.1 \pm 13.5 \text{ ng m}^{-3}$ ) before the LCD. Such differences in the molecular characteristics and aging level of diacids and related compounds before and during the LCD indicate substantially different formation pathways and influencing factors during these two observation periods, which will be discussed in more detail in Sections 3.3 and 3.4.

### 3.3 The aqueous-phase formation of diacids and related species before the LCD

As discussed above, the nighttime concentrations of  $C_2$ , diacids, and TDOCs exhibited higher values than those during the daytime. Such diurnal variations may be ascribed to the descended planetary boundary layer (PBL) height at night, which can cause enhanced concentrations of  $C_2$  and related SOA. However, the increase in the ratios of  $C_2$ /diacids and  $C_2$ /TDOCs at night indicated that the effect of lowered nighttime PBL height was minor, which could be supported by the insignificant diurnal differences of primary pollutant markers such as  $Na^+$ ,  $Ca^{2+}$ , and  $Mg^{2+}$  ( $p > 0.05$ , Table S3) between the daytime and



320 nighttime. Considering the higher RH and LWC concentration at night, the increased concentrations of  $C_2$  and related SOA during the nighttime may be closely linked to accelerated aqueous production (Cheng et al., 2015; Meng et al., 2020). The molecular pattern of TDOCs was predominated by  $C_2$  followed by  $C_4$  and  $C_3$  as discussed above, consistent with the molecular distribution in biomass burning smoke (Kawamura et al., 2013; Kundu et al., 2010; Meng et al., 2020; Sorathia et al., 2018). To explore the contribution of biomass burning to TDOCs, levoglucosan, and  $K^+$  were proposed as reliable markers for biomass burning (Hoffmann et al., 2010; Huang et al., 2006).  $K^+$  is abundant in aerosols emitted from biomass burning (Andreae, 1983), thus  $K^+$  exhibited a close correlation with levoglucosan ( $R^2=0.77$ , Table S1) before the LCD. There was no obvious diurnal difference of levoglucosan and  $K^+$  between daytime ( $140 \pm 54.9 \text{ ng m}^{-3}$ ,  $2.0 \pm 0.1 \text{ } \mu\text{g m}^{-3}$ ) and nighttime ( $141 \pm 84.4 \text{ ng m}^{-3}$ ,  $2.1 \pm 0.4 \text{ } \mu\text{g m}^{-3}$ ), suggesting that the higher concentrations of  $C_2$  and related SOA at night were irrelevant to the difference in the emission strength of organic precursors from biomass burning in the daytime and nighttime.  $C_2$ , diacids, and TDOCs exhibited strong correlations with levoglucosan and  $K^+$  before the LCD ( $R^2 > 0.5$ ), while such correlations were not observed during the LCD ( $R^2 < 0.2$ , Table S1), suggesting that biomass burning was an essential contributor to  $C_2$  and related SOA before the LCD rather than during the LCD. The ratio of  $C_2$ /levoglucosan ( $1.7 \pm 0.6$ ) at night before the LCD exhibited a larger value than that ( $1.3 \pm 0.5$ ) in the day, which was mainly ascribed to the accelerated aqueous formation of  $C_2$  at night. Moreover, the mean values of  $C_2$ /levoglucosan ( $1.5 \pm 0.6$ ),  $C_2/K^+$  ( $0.2 \pm 0.03$ ),  $C_4$ /levoglucosan ( $0.4 \pm 0.1$ ), and  $C_4/K^+$  ( $0.05 \pm 0.02$ ) ratios before the LCD were higher than those (0.05, 0.05, 0.03, and 0.03) in fresh particles emitted from savanna fires of southern African (Gao et al., 2003). It is interesting to note that the average ratios of  $C_2/C_4$  ( $3.9 \pm 1.5$ ),  $C_3/C_4$  ( $0.3 \pm 0.1$ ), and  $C_2$ /diacids ( $0.52 \pm 0.55$ ) before the LCD were almost equal to those (3.8, 0.3, and 0.55) measured in the aerosols for two days aging biomass samples via chamber experiments (Shen et al., 2022), suggesting that  $C_2$  and related SOA before the LCD were linked tightly to the secondary oxidation of organic precursors emitted from biomass burning.

340 To explore the formation pathways and contributing factors of  $C_2$  and related SOA before the LCD, the temporal variations of major diacids, LWC,  $\text{pH}_{\text{is}}$ , and meteorological parameters (e.g., solar radiation, temperature, and RH) were illustrated in Fig. 5. The  $\text{SO}_4^{2-}$  formation was largely from aqueous phase oxidation (see Text S5), thus the correlation analysis between  $\text{SO}_4^{2-}$  and  $C_2$  can be used to evaluate the formation process of  $C_2$  mainly via aqueous phase pathways (Sorathia et al., 2018).  $C_2$  was correlated significantly with  $\text{SO}_4^{2-}$  in the daytime ( $R^2 = 0.53$ ) and nighttime ( $R^2 = 0.66$ ) (Fig. S2) before the LCD, confirming the dominant aqueous-phase formation pathway of  $C_2$ . It is worth noting that the slope of the regression line of the  $C_2/\text{SO}_4^{2-}$  ratio (0.005) at night was 1.3 times higher than that (0.004) during the daytime (Fig. S2). Both the higher slope and  $C_2$  concentrations indicate a more efficient formation of  $C_2$  at night, largely because the  $C_2$  production requires multiple steps of aqueous oxidation from VOCs while the formation of  $\text{SO}_4^{2-}$  requires fewer steps (Miyazaki et al., 2009). Noticeably, the concentrations of  $C_2$  and diacids, as well as the  $C_2$ /diacids ratio culminated on the nighttime of January 23, which was characterized by significantly higher LWC concentration ( $172 \text{ } \mu\text{g m}^{-3}$ ) and RH (86.9%) (Fig. 5). Gly and mGly are gaseous oxidation products of biogenic and anthropogenic VOCs with OH· radicals, and both are highly water-soluble and thus can dissolve in the aqueous phase (Carlton et al., 2006; Myriokefalitakis et al., 2011). The correlations of the concentrations of Gly, mGly, and  $C_2$  with OH· radicals were not straightforward ( $p > 0.05$ , Fig. S4), primarily because of the multiple sources (e.g., biomass burning, fossil fuel combustion, and other sources except for the aqueous OH· radical oxidation pathway) of  $C_2$  (Cao et al., 2017; Narukawa et al., 1999; Xu et al., 2022) and the complexity of the local atmospheric environment. In addition, the concentrations of each component varied continuously with their molar fractions in the aerosol phase during the reaction process, thus  $C_2$  was not necessarily correlated directly with OH· radicals. The higher RH and LWC concentration were favorable for the partitioning of Gly and mGly from a gaseous phase to an aqueous phase and forming  $C_2$ . As shown in Fig. 5, the enhanced concentrations of Gly and mGly in  $\text{PM}_{2.5}$  before the LCD were observed when RH and LWC increased. Thus,  $C_2$  and its precursors (including Gly and mGly) were positively correlated with RH and LWC, respectively ( $R^2 > 0.45$ , Fig. 4a). Moreover, the ratios of  $C_2$ /Gly and  $C_2$ /mGly also showed a significant correlation with RH and LWC ( $R^2 > 0.4$ , Fig.

360

4a). Indeed, the increase in  $C_2$  (increased by 1.9 times) was significantly higher than that of Gly (increased by 1.1 times) and mGly (increased by 1.2 times) with the increase of LWC before the LCD. These discussions suggest that the higher LWC concentration and RH could promote the aqueous-phase formation of  $C_2$  from Gly and mGly. Therefore,  $C_2$  before the LCD was mainly derived from the aqueous production where LWC and RH appeared to be vitally important controlling factors as supported by positive matrix factorization (PMF) results that will be discussed in Section 3.6. The nighttime concentrations of LWC and RH were higher than those during the daytime, which led to the higher concentration and percentage contribution of  $C_2$  in the nighttime.

Previous studies have reported that  $C_2$  can also be derived from the chain-breaking of longer-chain diacids in the aqueous phase (Kawamura and Usukura, 1993; Miyazaki et al., 2009). However, there was moderate or no serious correlation between  $C_2$  and longer-chain diacids (e.g.,  $C_3$  and  $C_4$ ), respectively ( $R^2 < 0.3$ , Fig. 4a). Furthermore, longer-chain diacids and the ratios of  $C_2/C_3$  and  $C_2/C_4$  exhibited no significant correlation with LWC or RH ( $R^2 < 0.24$ , Fig. 4a). It can be concluded the effect of chain-breaking of longer homologous diacids on aqueous mechanism of  $C_2$  was negligible in this study. Numerous studies have reported that the acidic condition of aerosol is beneficial to the BSOA formation such as 2-methylglyceric acid from BVOCs (e.g., isoprene), and ultimately be transformed into  $C_2$  via Gly, mGly, and  $\omega C_2$  in the aqueous phase by acid-catalyzed oxidation reactions (Surratt et al., 2007). Laboratory experiment has pointed out that the acidic environment of aerosol can accelerate the uptake and production of Gly and mGly via acidic-catalyzed heterogeneous oxidation (Jang et al., 2002; Surratt et al., 2007). As shown in Fig. 4a,  $pH_{is}$  exhibited pronounced negative relationships with  $C_2$  and its precursors such as Gly and mGly ( $R^2 \geq 0.45$ ), which was also found in other field studies (Cheng et al., 2017; Meng et al., 2014; Wang et al., 2017; Yu et al., 2021), possibly suggesting an acid-catalyzed  $C_2$  formation in the aqueous phase under the present atmospheric conditions before the LCD. However, Tan et al. (2009) reported that acidity had a minor effect on  $C_2$  formation at cloud- and fog-relevant conditions via online experiments. Wang et al. (2015) suggested that the coarse particles during the dust period, which are alkaline, are favorable for the  $C_2$  formation from  $\omega C_2$ , largely because the reaction rate constant ( $3.6 \times 10^8 \text{ M}^{-1} \text{ s}^{-1}$ ) of  $\omega C_2$  with  $\text{OH} \cdot$  radical to form  $C_2$  is smaller than that ( $2.9 \times 10^9 \text{ M}^{-1} \text{ s}^{-1}$ ) of its anion, glyoxylate. At very acidic pH,  $C_2$  is not only formed more slowly but also oxidized more slowly (Eugene et al., 2016; Herrmann, 2003). Those findings conflicted with each other, probably because the concentration levels of organic precursors, acidity, LWC, and other influencing factors were different from the cases in our field observations, thus further studies are necessary to elucidate the influencing mechanism of acidity on  $C_2$  formation.

### 3.4 Enhanced gaseous photochemical formation of diacids and related species during the LCD

Being different from the time period before the LCD, the strong correlations of  $C_2$ , Gly, mGly, and ratios of  $C_2/\text{Gly}$  and  $C_2/\text{mGly}$  were not obtained with RH or LWC ( $R^2 < 0.2$ ) during the LCD (Fig. 4b), suggesting the insignificant effect of the aqueous-phase formation on  $C_2$  during the LCD. As discussed in Section 3.2, the concentrations of  $C_2$ , diacids, and TDOCs as well as the ratio of  $C_2/\text{diacids}$  during the LCD were higher than those before the LCD, despite the anthropogenic source strength dropping dramatically during the LCD. Given the higher  $\text{O}_3$  concentration and stronger solar radiation during the LCD (Table 1), it can be expected that the enhanced concentration and contribution of  $C_2$  were driven by the promoted photochemical oxidation, which was supported by the significantly higher  $C_3/C_4$  ratio ( $1.6 \pm 0.4$ ) during the LCD than that ( $0.3 \pm 0.1$ ) before the LCD. Since  $C_3$  can be generated from photochemical oxidation of  $C_4$  in the atmosphere (Kawamura and Bikkina, 2016), the relatively high  $C_3/C_4$  ratio during the LCD (Fig. 3b) indicates that aerosols during the LCD experienced more substantial photochemical aging. Field measurements and chamber experiments have reported that  $C_2$  can principally originate from photochemical oxidation of  $\alpha$ -dicarbonyls from VOCs driven by  $\text{O}_3$  and  $\text{OH} \cdot$  radicals (Meng et al., 2021; Mochizuki et al., 2017). Bikkina et al. (2021) reported a laboratory production of  $C_2$  and other LMW diacids together with intermediate oxoacids and  $\alpha$ -dicarbonyls by ozonolysis of isoprene.  $\text{O}_3$  was used here as a marker for the oxidant

405 concentration of gaseous photochemical oxidation. In addition, solar radiation could also be used as a reliable proxy for gaseous photochemical productions of  $C_2$  and other diacids (Deshmukh et al., 2018). In view of the significant enhancement of oxidant concentration (e.g.,  $O_3$  and  $OH \cdot$  radicals) and solar radiation during the LCD, it could be concluded that the production of  $C_2$  and related compounds may be driven by the higher oxidant concentrations.

To investigate the formation mechanism and potential sources of  $C_2$  and related compounds during the LCD, the temporal variations in  $C_2$  and its precursors,  $O_3$ , as well as meteorological factors are presented in Fig. 5. It is interesting to note that the highest  $O_3$  concentration was observed on the daytime of January 31 when the concentrations of  $C_2$  and diacids reached their peaks. Moreover, both  $C_2$  and diacids concentrations as well as the  $C_2$ /diacids ratio exhibited robust correlations with  $O_3$  ( $R^2 > 0.5$ , Fig. 4b), respectively, suggesting that  $O_3$  or related oxidants may have played an important role in the formation of  $C_2$  and other diacids. Additionally,  $C_2$  and diacids concentrations exhibited similar patterns of variations (Fig. 5) and strong correlations ( $R^2 > 0.5$ , Fig. 4b) with solar radiation during the daytime. However, such similarities and strong correlations were not observed with temperature ( $R^2 < 0.2$ , Fig. 4b and Fig. 5), again suggesting that the effect of temperature on the loss of  $C_2$  and diacids was negligible. These results confirmed that  $C_2$  and other diacids were overwhelmingly derived from the gaseous photochemical processes driven by the stronger solar radiation,  $O_3$ , and other oxidants such as  $OH \cdot$  radicals.

A number of studies have demonstrated that the longer-chain diacids can be photochemically degraded into  $C_2$  (Kawamura and Bikkina, 2016; Zhao et al., 2020). It is worth noting that  $C_2$  was correlated strongly with longer-chain diacids such as  $C_3$  and  $C_4$ , respectively ( $R^2 > 0.5$ , Fig. 4b). The ratio of  $C_2$ /diacids was correlated strongly with the ratios of  $C_3/C_4$  ( $R^2 = 0.68$ ) and  $C_2/C_4$  ( $R^2 = 0.58$ , Fig. 4b), indicating that  $C_2$  during the LCD may be largely derived from the photochemical degradation of higher molecular weight homologues of diacids. However, the correlation of the  $C_2$ /diacids ratio with  $(C_3-C_{11})-C/WSOC$  ( $R^2 = 0.12$ ) was weak, primarily because the supply rates of longer-chain diacids are faster than their degradation rates in  $C_2$  formation (Zhao et al., 2020).  $C_2$ /diacids ratio was correlated robustly with solar radiation during the daytime ( $R^2 = 0.76$ , Fig. 4b). Previous study suggested that the correlation analysis of  $C_2$ /diacids,  $C_2/C_4$ , and  $C_3/C_4$  with  $O_3$  could indicate the photochemical chain-breaking of longer-chain diacids producing  $C_2$  (Liu et al., 2021). These ratios were observed to be correlated significantly with  $O_3$  ( $R^2 > 0.45$ , Fig. 4b). These results confirm that  $C_2$  during the LCD primarily originated from the photochemical degradation of longer-chain homologous diacids driven by stronger solar radiation and higher  $O_3$  concentration and other oxidants rather than higher temperature, which was further supported by the results of stable carbon isotopic composition of diacids (discussed in Section 3.5) and PMF analysis (discussed in Section 3.6).

### 3.5 Stable carbon isotopic compositions of diacids and related species before and during the LCD

The  $\delta^{13}C$  values of specific organic acids can provide insights into the sources and photochemical aging (or processing) of organic aerosols due to the isotopic fractionation of carbon during the phase partitioning and/or photochemical oxidation (Wang et al., 2020a; Zhang et al., 2016). Thus, we investigated the stable carbon isotopic compositions of major diacid homologues to further discuss the atmospheric processes of diacid homologues and evaluate the aging degree of organic aerosols before and during the LCD.

On average, most of the detected diacid homologues exhibited higher  $\delta^{13}C$  values during the LCD than those before the LCD (Table 3, Fig. 6). A previous study demonstrated that the enriched  $\delta^{13}C$  values in diacid homologues were found with UV irradiation time (Pavuluri and Kawamura, 2016). Additionally, Shen et al. (2022) reported that the  $\delta^{13}C$  value of  $C_2$  in the 7-d aged biomass samples was higher than in the 2-d aged biomass samples using the combustion chamber. Thus, the enrichment of  $\delta^{13}C$  values in diacid homologues during the LCD was mainly due to the promoted photochemical oxidation during the LCD. Similar to the diurnal variations in major diacids' concentrations, the nighttime  $\delta^{13}C$  values of these detected diacids were more positive (or more negative) than those in the daytime before (or during) the LCD, which was ascribed to their different sources and formation processes in these two observation periods. In brief, the  $\delta^{13}C$  values

exhibited a decreasing trend as the carbon numbers of diacids increased (Fig. 6), consistent with other observation campaigns elsewhere (Meng et al., 2020; Pavuluri and Kawamura, 2016; Wang and Kawamura, 2006). The mean  $\delta^{13}\text{C}$  value ( $-20 \pm 2.5\%$ ) of  $\text{C}_2$  was the highest in each period (Table 3), which was comparable to that ( $-20 \pm 3.5\%$ ) observed in its surrounding city such as Liaocheng (Meng et al., 2020), and higher than the values obtained in other China's megacities such as Beijing ( $-23 \pm 3.4\%$ ) (Zhao et al., 2018) and Xi'an ( $\text{PM}_{2.1}$ : from  $-21$  to  $-24\%$ ) (Wang et al., 2012), but smaller than the values measured in the Korea Climate Observatory at Gosan ( $-16 \pm 4.3\%$ ) of East Asia (Zhang et al., 2016) and western Pacific and Southern Ocean ( $-17 \pm 0.8\%$ ) (Wang and Kawamura, 2006) in the winter (Fig. 7). It is worth noting that the average  $\delta^{13}\text{C}$  value of  $\text{C}_2$  ( $-22 \pm 1.9\%$ ) before the LCD was equal to that ( $-22 \pm 1.2\%$ ) determined in the 2-d biomass samples (Shen et al., 2022) (Fig. 7), confirming that biomass burning and subsequent oxidation exerted an important effect on  $\text{C}_2$  before the LCD.

As mentioned above,  $\text{C}_2$  can not only originate from the photochemical breakdown (or decomposition) of  $\text{C}_3$  and  $\text{C}_4$  via  $\text{kC}_3$  and hydroxymalonic acids ( $\text{hC}_4$ ) but also be derived from the photochemical oxidation of aromatic hydrocarbons via  $\omega\text{C}_2$ . The positive correlations of the  $^{13}\text{C}$  values of  $\text{C}_2$  with mass ratios of  $\text{C}_2/\omega\text{C}_2$  ( $R^2 \geq 0.39$ ) and  $\text{C}_2/\text{kC}_3$  ( $R^2 \geq 0.37$ ) during the LCD were observed, whereas such robust relations only with  $\text{C}_2/\omega\text{C}_2$  ( $R^2 \geq 0.47$ ) rather than  $\text{C}_2/\text{kC}_3$  ( $R^2 \geq 0.01$ ) before the LCD were observed (Fig. 8). These results imply that the effect of photochemical decomposition of higher diacid homologues on  $\text{C}_2$  before the LCD was minor, consistent with the discussions in Section 3.3. The isotopic values of diacids followed the order of  $\text{C}_2 > \text{C}_3 > \text{C}_4$  in each time period (Fig. 6), primarily because diacids containing more carbon numbers may be more reactive to oxidants such as  $\text{O}_3$  and  $\text{OH}$  radicals in the atmosphere (Aggarwal and Kawamura, 2008). On the other hand, the removal of  $\text{CO}_2/\text{CO}$  in the processes of  $\text{C}_3$  and  $\text{C}_4$  reacting with atmospheric oxidants can generate more  $^{13}\text{C}$ -enriched  $\text{C}_2$  due to the KIEs (Wang and Kawamura, 2006). The isotopic values of  $\text{C}_9$  ranged from  $-25$  to  $-30\%$  before the LCD, whose difference was less distinguished than those of  $\text{C}_2$ - $\text{C}_4$  (Table 3). It is worth noting that the  $\delta^{13}\text{C}$  values of organic species from marine plankton ( $-20\%$ ) are higher than those from terrestrial higher plants ( $\text{C}_3$  plants:  $-27\%$ ). The  $\delta^{13}\text{C}$  values of  $\text{C}_9$  and the strong correlation of  $\text{C}_9$  with levoglucosan before the LCD as discussed above indicate that biomass burning emitting unsaturated fatty acids and subsequent aqueous oxidation was an important contributor to  $\text{C}_9$  in Jinan during the wintertime. The most negative  $\delta^{13}\text{C}$  value among the identified organic species was tPh throughout the entire period, whose  $\delta^{13}\text{C}$  value ( $-35 \pm 3.1\%$ ) was approximately equal to that ( $-35 \pm 5.3\%$ ) in Liaocheng (Meng et al., 2020) and lighter than that ( $-34 \pm 3.4\%$ ) in Beijing (Zhao et al., 2018) of China where the primary emissions from the combustion of plastic wastes is an essential source of tPh. Moreover, the  $\delta^{13}\text{C}$  value of tPh was negatively (one outlier that possessed a relatively high relative abundance of tPh in diacids was removed) in the daytime or poorly correlated with the ratio of tPh/diacids at night before the LCD (Fig. 8f). The  $\delta^{13}\text{C}$  value of tPh presented a negative correlation with the tPh/diacids during the LCD (Fig. 8i). These results suggest that the primary sources of plastic wastes burning exerted a significant impact on tPh in the atmosphere of Jinan.

Similarly, the  $\delta^{13}\text{C}$  value of oxoacids increases as carbon number decreases (Table 3, Fig. 6).  $\omega\text{C}_2$  has the highest  $\delta^{13}\text{C}$  value, followed by Pyr, and  $\omega\text{C}_3$  before and during the LCD. The lighter isotope ( $^{12}\text{C}$ ) was more enriched in  $\omega\text{C}_2$  than both Gly and mGly (Table 3) in each time period.  $\omega\text{C}_2$  is largely derived from the photochemical oxidation of organic precursors such as  $\alpha$ -dicarbonyls and acetic acid (Carlton et al., 2007).  $^{12}\text{C}$  can be preferentially accumulated in the products in the non-reversible chemical processes (Wang et al., 2012), resulting in the lighter  $\delta^{13}\text{C}$  values of  $\omega\text{C}_2$  than its precursors. mGly was less enriched in  $^{13}\text{C}$  than Gly (Table 3, Fig. 6) in each time period, attributed to the lower vapor pressure and higher carbon numbers of mGly that may lead to the weaker isotopic fractionation (Zhang et al., 2016).

It is well established that the  $^{13}\text{C}$  values of diacids and related compounds become isotopically heavier in the aging process of organic aerosols (Pavuluri and Kawamura, 2016; Zhang et al., 2016). As mentioned above, the ratios of  $\text{C}_2/\text{Gly}$ ,  $\text{C}_2/\text{mGly}$ , and  $\text{C}_2/\text{diacids}$  are usually considered significant proxies to evaluate the aging of organic aerosols. These ratios exhibited strong correlations with the  $^{13}\text{C}$  values of  $\text{C}_2$  in each period ( $R^2 > 0.4$ , Fig. 8), indicating the production of more  $^{13}\text{C}$ -enriched

C<sub>2</sub> during the aging processes. The less depletion of <sup>13</sup>C in C<sub>2</sub> of aged organic aerosols conformed to the actual secondary KIE on activated H-atom abstraction by OH radicals rather than to the mass dependence of collision frequencies in the gas phase (Enami et al., 2015). Organic species can react with OH radicals and other atmospheric oxidants in the atmospheric oxidation reactions, which result in the removal of CO<sub>2</sub>/CO containing <sup>12</sup>C and cause the oxidation products more enriched with the heavier isotope <sup>13</sup>C (Narukawa et al., 1999). Therefore, the <sup>13</sup>C values of major diacids and the related compounds during the LCD were less negative than those before the LCD, again demonstrating that the gaseous photochemical oxidation was promoted during the LCD because of the higher temperature and O<sub>3</sub> concentration under the clearer sky conditions, which was in agreement with the results in Section 3.2.

### 3.6 Comparison of the source fingerprinting before and during the LCD

To further quantitatively analyze the crucial sources and their relative contributions to diacids and related compounds, PMF was adopted. Detailed information about PMF analysis was described in Text S3. The model stability of the five-factor solution and error estimation diagnostics were detailed in Table S5 and Table S6, respectively. The PMF-resolved source profiles for the five factors before and during the LCD are shown in Fig. 9. Before the LCD, C<sub>2</sub>, C<sub>3</sub>, ωC<sub>2</sub>, Pyr, Gly, mGly, LWC, WSOC, NO<sub>3</sub><sup>-</sup>, SO<sub>4</sub><sup>2-</sup>, and NH<sub>4</sub><sup>+</sup> exhibited the relatively higher loadings in the first factor (Fig. 9a). SO<sub>4</sub><sup>2-</sup> is a representative product of secondary oxidation in the aqueous phase, and LWC had been proved to be a significant influencing factor during the aqueous oxidation as discussed above. Therefore, the first factor was considered the sources from aqueous phase oxidation. The second factor was characterized by the stronger loadings of C<sub>3</sub>, C<sub>4</sub>, Ph, and EC. Ph is generated from the photochemical oxidation of polycyclic aromatic hydrocarbons (e.g., naphthalene) that are primarily emitted from the domestic coal combustion in China's megacities (Zhao et al., 2018), thus the second factor was categorized as a coal combustion source. O<sub>3</sub> had been confirmed to be a reliable proxy for gaseous photochemical oxidation, thus the robust relationships of O<sub>3</sub>, α-dicarbonyls, and ωC<sub>2</sub> with the third factor indicated the contribution of gaseous photochemical oxidation. The fourth factor was significantly associated with Mg<sup>2+</sup> and Ca<sup>2+</sup>, which represented dust emission. As an important indicator of biomass burning, levoglucosan was strongly correlated with C<sub>9</sub> and EC in the fifth factor. Although diacids and related compounds can be produced from the secondary oxidation of organic precursors from biomass burning (Cao et al., 2017; Kawamura et al., 2013), biomass burning can directly emit those compounds (Fu et al., 2008; Gao et al., 2003; Kundu et al., 2010; Narukawa et al., 1999; Shen et al., 2022). Thus, the fifth factor could be regarded as a primary source of biomass burning.

During the LCD, the first factor was dominated by O<sub>3</sub>, major diacids, and α-dicarbonyls (Fig. 9b), which represented gaseous photochemical oxidation. The second factor was strongly correlated with C<sub>2</sub>, C<sub>4</sub>, LWC, WSOC, NO<sub>3</sub><sup>-</sup>, SO<sub>4</sub><sup>2-</sup>, and NH<sub>4</sub><sup>+</sup>, suggesting a significant contribution of aqueous oxidation. Levoglucosan, C<sub>9</sub>, EC, and OC presented stronger loadings in the third factor, indicating a primary source of biomass burning. Mg<sup>2+</sup> and Ca<sup>2+</sup> exhibited strong correlations with the fourth factor, suggesting the sources from dust emission. Ph and EC presented strong correlations with the fifth factor, representing a coal combustion source. The PMF-resolved relative contributions to the detected species before and during the LCD were presented in Fig. 9c and Fig. 9d, respectively. The aqueous oxidation made the greatest contribution (47.2%) to C<sub>2</sub> and related compounds, while the gaseous photochemical oxidation contributed only 12.3% to the total determined sources before the LCD, again suggesting that the aqueous oxidation was the dominant formation pathway for these organic compounds before the LCD as discussed in Section 3.3. However, the gaseous photochemical oxidation contributed the largest percentage (50.5%) to the total identified sources, while the aqueous oxidation accounted for only 16.1% of the total identified sources during the LCD, confirming that the gaseous photochemical oxidation exerted a leading role in the formation of homologous diacids during the LCD, which was in agreement with the results as discussed in Section 3.4. The lower contribution of C<sub>2</sub> and related compounds from aqueous oxidation during the LCD was likely because of the decrease of RH and LWC. The contribution of biomass burning increased from 11.4% before the LCD to 13.6% during the LCD.

However, the contribution of coal combustion decreased from 16.2% before the LCD to 7.2% during the LCD, largely because of the decreased usage of coal for the industry.

#### 4 Summary and conclusions

535 This work has investigated the effects of variations in anthropogenic emissions and meteorological conditions on the formation pathways and influencing factors of diacids and related compounds by taking advantage of COVID-19 LCD as a “controlled experiment”. Previous studies focused on the relationships of higher diacids and related compounds with more source emissions or/and promoted secondary oxidation. However, this study strongly suggested that the secondary formation of diacids and related species was enhanced despite the significant decline of organic precursors from anthropogenic pollutant emissions during the LCD. Before the LCD, higher RH and hygroscopic particles (e.g., SIA) led to an increase in LWC, which promoted the partitioning of water-soluble organic precursors (e.g., Gly and mGly) from the gaseous phase into the aqueous phase, thereby enhancing the aqueous formation of C<sub>2</sub> (Fig. 10). During the LCD, C<sub>2</sub> was derived from the photochemical degradation of longer-chain diacids (e.g., C<sub>3</sub> and C<sub>4</sub>) that was driven by the stronger solar radiation and higher O<sub>3</sub> concentration and other oxidants (Fig. 10).  
540

In this study, we quantified the relative contributions of aqueous-phase oxidation and gaseous-phase photochemical oxidation to the ambient C<sub>2</sub> and related species, which were 47.2% and 12.3% before the LCD and 16.1% and 50.5% during the LCD, respectively. Moreover, the δ<sup>13</sup>C values of C<sub>2</sub> during the LCD were higher than those before the LCD (Fig. 10), largely because the reactivity of <sup>13</sup>C was higher than that of <sup>12</sup>C in the gaseous photochemical oxidation. We also observed more enriched <sup>13</sup>C in C<sub>2</sub> during the aging processes of organic aerosols. C<sub>2</sub> was not necessarily correlated directly with OH· radicals in the aqueous oxidation, possibly due to the fact that C<sub>2</sub> has multiple sources (e.g., biomass burning and fossil fuel combustion) and the complexity of the local atmospheric environment, which still needs to be elucidated by more field observations. These results are helpful for better understanding the sources, formation processes, and driving factors of SOA in the urban regions of East China. Nevertheless, our study suggested that, even if the primary emissions are practically reduced, we cannot completely solve the current air pollution problem in the North China Plain where the sources and precursors of secondary aerosols are extremely complicated. The balanced strategy and trans-regional joint control of major air pollutants are necessary to be considered together with meteorological conditions.  
545  
550  
555

Overall, we obtained that the sources, formation mechanisms, and aging processes of SOA differed significantly during different time periods even at the same observation site. It is needed to conduct more field observations of SOA regarding the types of precursors, formation pathway via aqueous oxidation and gaseous photochemical oxidation, and aging level at different sites and in different time periods to improve the accuracy of aerosol models and informing policy about effective air quality measures.  
560

*Data availability.* The data in this study are available at: <https://doi.org/10.5281/zenodo.7533247> (Meng et al., 2023).

*Author contribution.* PF designed the study. YW, YL, TH, and MC carried out the experiments and performed the data analysis. HZ and KL estimated the OH · radical concentration. JM prepared the manuscript with contributions from all co-authors.

565 *Competing interests.* The authors have the following competing interests: One of the coauthors, Prof. Kimitaka Kawamura is one of the editorial members of this journal.

570 *Acknowledgments.* This work was supported by the National Natural Science Foundation of China (Grant No. 42177083), the Natural Science Foundation of Shandong Province (Grant No. ZR2020MD113), the Junior Faculty Support Program for Scientific and Technological Innovations in Shandong Provincial Higher Education Institutions (2021KJ085), and the Open Funds of State Key Laboratory of Loess and Quaternary Geology, Institute of Earth Environment, Chinese Academy of Sciences (Grant No. SKLLOG2020).

## References

- Aggarwal, S. G. and Kawamura, K.: Molecular distributions and stable carbon isotopic compositions of dicarboxylic acids and related compounds in aerosols from Sapporo, Japan: Implications for photochemical aging during long-range atmospheric transport, *J. Geophys. Res. Atmos.*, 113, D14301, [10.1029/2007jd009365](https://doi.org/10.1029/2007jd009365), 2008.
- 575 Andreae, M. O.: Soot Carbon and Excess Fine Potassium: Long-Range Transport of Combustion-Derived Aerosols, *Science*, 220, 1148, 1983.
- Bao, R. and Zhang, A.: Does lockdown reduce air pollution? Evidence from 44 cities in northern China, *Sci. Total Environ.*, 731, 139052, <https://doi.org/10.1016/j.scitotenv.2020.139052>, 2020.
- Bikkina, S., Kawamura, K., and Miyazaki, Y.: Latitudinal distributions of atmospheric dicarboxylic acids, oxocarboxylic acids, and  $\alpha$ -dicarbonyls over the western North Pacific: Sources and formation pathways, *J. Geophys. Res. Atmos.*, 120, 5010-5035, [10.1002/2014jd022235](https://doi.org/10.1002/2014jd022235), 2015.
- 580 Bikkina, S., Kawamura, K., Sakamoto, Y., and Hirokawa, J.: Low molecular weight dicarboxylic acids, oxocarboxylic acids and  $\alpha$ -dicarbonyls as ozonolysis products of isoprene: Implication for the gaseous-phase formation of secondary organic aerosols, *Sci. Total Environ.*, 769, 144472, <https://doi.org/10.1016/j.scitotenv.2020.144472>, 2021.
- 585 Cao, F., Zhang, S.-C., Kawamura, K., Liu, X., Yang, C., Xu, Z., Fan, M., Zhang, W., Bao, M., Chang, Y., Song, W., Liu, S., Lee, X., Li, J., Zhang, G., and Zhang, Y.-L.: Chemical characteristics of dicarboxylic acids and related organic compounds in PM<sub>2.5</sub> during biomass-burning and non-biomass-burning seasons at a rural site of Northeast China, *Environ. Pollut.*, 231, 654-662, <https://doi.org/10.1016/j.envpol.2017.08.045>, 2017.
- 590 Carlton, A. G., Turpin, B. J., Lim, H.-J., Altieri, K. E., and Seitzinger, S.: Link between isoprene and secondary organic aerosol (SOA): Pyruvic acid oxidation yields low volatility organic acids in clouds, *Geophys. Res. Lett.*, 33, L06822, [10.1029/2005gl025374](https://doi.org/10.1029/2005gl025374), 2006.
- Carlton, A. G., Turpin, B. J., Altieri, K. E., Seitzinger, S., Reff, A., Lim, H.-J., and Ervens, B.: Atmospheric oxalic acid and SOA production from glyoxal: Results of aqueous photooxidation experiments, *Atmos. Environ.*, 41, 7588-7602, <http://dx.doi.org/10.1016/j.atmosenv.2007.05.035>, 2007.
- 595 Chen, S., Xie, Q. R., Su, S. H., Wu, L. B., Zhong, S. J., Zhang, Z. M., Ma, C., Qi, Y. L., Hu, W., Deng, J. J., Ren, L. J., Zhu, D. Q., Guo, Q. J., Liu, C. Q., Jang, K. S., and Fu, P. Q.: Source and formation process impact the chemodiversity of rainwater dissolved organic matter along the Yangtze River Basin in summer, *Water Research*, 211, 118024, [10.1016/j.watres.2021.118024](https://doi.org/10.1016/j.watres.2021.118024), 2022.
- 600 Cheng, C., Li, M., Chan, C. K., Tong, H., Chen, C., Chen, D., Wu, D., Li, L., Wu, C., Cheng, P., Gao, W., Huang, Z., Li, X., Zhang, Z., Fu, Z., Bi, Y., and Zhou, Z.: Mixing state of oxalic acid containing particles in the rural area of Pearl River Delta, China: implications for the formation mechanism of oxalic acid, *Atmos. Chem. Phys.*, 17, 9519-9533,

10.5194/acp-17-9519-2017, 2017.

- Cheng, C., Wang, G., Meng, J., Wang, Q., Cao, J., Li, J., and Wang, J.: Size-resolved airborne particulate oxalic and related secondary organic aerosol species in the urban atmosphere of Chengdu, China, *Atmos. Res.*, 161–162, 134–142, <http://dx.doi.org/10.1016/j.atmosres.2015.04.010>, 2015.
- Cheng, C., Wang, G., Zhou, B., Meng, J., Li, J., Cao, J., and Xiao, S.: Comparison of dicarboxylic acids and related compounds in aerosol samples collected in Xi'an, China during haze and clean periods, *Atmospheric Environment*, 81, 443–449, <http://dx.doi.org/10.1016/j.atmosenv.2013.09.013>, 2013.
- Chow, J. C., Watson, J. G., Chen, L. W. A., Arnott, W. P., Moosmüller, H., and Fung, K.: Equivalence of Elemental Carbon by Thermal/Optical Reflectance and Transmittance with Different Temperature Protocols, *Environ. Sci. Technol.*, 38, 4414–4422, [10.1021/es034936u](https://doi.org/10.1021/es034936u), 2004.
- Crahan, K. K., Hegg, D., Covert, D. S., and Jonsson, H.: An exploration of aqueous oxalic acid production in the coastal marine atmosphere, *Atmospheric Environment*, 38, 3757–3764, <http://dx.doi.org/10.1016/j.atmosenv.2004.04.009>, 2004.
- Deshmukh, D. K., Mozammel Haque, M., Kawamura, K., and Kim, Y.: Dicarboxylic acids, oxocarboxylic acids and  $\alpha$ -dicarbonyls in fine aerosols over central Alaska: Implications for sources and atmospheric processes, *Atmos. Res.*, 202, 128–139, <https://doi.org/10.1016/j.atmosres.2017.11.003>, 2018.
- Devineni, S. R., Pavuluri, C. M., Wang, S., Ren, L., Xu, Z., Li, P., Fu, P., and Liu, C.-Q.: Size-Resolved Characteristics and Sources of Inorganic Ions, Carbonaceous Components and Dicarboxylic Acids, Benzoic Acid, Oxocarboxylic Acids and  $\alpha$ -Dicarbonyls in Wintertime Aerosols from Tianjin, North China, *Aerosol Science and Engineering*, 7, 1–22, [10.1007/s41810-022-00159-0](https://doi.org/10.1007/s41810-022-00159-0), 2023.
- Ding, Z., Du, W., Wu, C., Cheng, C., Meng, J., Li, D., Ho, K., Zhang, L., and Wang, G.: Summertime atmospheric dicarboxylic acids and related SOA in the background region of Yangtze River Delta, China: Implications for heterogeneous reaction of oxalic acid with sea salts, *Sci. Total Environ.*, 757, 143741, <https://doi.org/10.1016/j.scitotenv.2020.143741>, 2021.
- Enami, S., Hoffmann, M. R., and Colussi, A. J.: Stepwise Oxidation of Aqueous Dicarboxylic Acids by Gas-Phase OH Radicals, *J. Phys., Chem. Lett.*, 6, 527–534, [10.1021/jz502432j](https://doi.org/10.1021/jz502432j), 2015.
- Ervens, B., Feingold, G., Frost, G. J., and Kreidenweis, S. M.: A modeling study of aqueous production of dicarboxylic acids: 1. Chemical pathways and speciated organic mass production, *J. Geophys. Res.*, 109, D15205, [10.1029/2003jd004387](https://doi.org/10.1029/2003jd004387), 2004.
- Ervens, B., Turpin, B. J., and Weber, R. J.: Secondary organic aerosol formation in cloud droplets and aqueous particles (aqSOA): a review of laboratory, field and model studies, *Atmos. Chem. Phys.*, 11, 11069–11102, [10.5194/acp-11-11069-2011](https://doi.org/10.5194/acp-11-11069-2011), 2011.
- Eugene, A. J., Xia, S.-S., and Guzman, M. I.: Aqueous Photochemistry of Glyoxylic Acid, *The Journal of Physical Chemistry A*, 120, 3817–3826, [10.1021/acs.jpca.6b00225](https://doi.org/10.1021/acs.jpca.6b00225), 2016.
- Fountoukis, C., and Nenes, A.: ISORROPIA II: a computationally efficient thermodynamic equilibrium model for  $\text{K}^+ - \text{Ca}^{2+} - \text{Mg}^{2+} - \text{NH}_4^+ - \text{Na}^+ - \text{SO}_4^{2-} - \text{NO}_3^- - \text{Cl}^- - \text{H}_2\text{O}$  aerosols, *Atmos. Chem. Phys.*, 7, 4639–4659, [10.5194/acp-7-4639-2007](https://doi.org/10.5194/acp-7-4639-2007), 2007.
- Fu, P., Kawamura, K., Usukura, K., and Miura, K.: Dicarboxylic acids, ketocarboxylic acids and glyoxal in the marine aerosols collected during a round-the-world cruise, *Marine Chemistry*, 148, 22–32, <http://dx.doi.org/10.1016/j.marchem.2012.11.002>, 2013.
- Fu, T.-M., Jacob, D. J., Wittrock, F., Burrows, J. P., Vrekoussis, M., and Henze, D. K.: Global budgets of atmospheric glyoxal and methylglyoxal, and implications for formation of secondary organic aerosols, *J. Geophys. Res.*, 113, D15303, [10.1029/2007jd009505](https://doi.org/10.1029/2007jd009505), 2008.



- 645 Gao, S., Hegg, D. A., Hobbs, P. V., Kirchstetter, T. W., Magi, B. I., and Sadilek, M.: Water-soluble organic components in aerosols associated with savanna fires in southern Africa: Identification, evolution, and distribution, *J. Geophys. Res. Atmos.*, 108, 8491, 10.1029/2002jd002324, 2003.
- Gaubert, B., Bouarar, I., Doumbia, T., Liu, Y., Stavrakou, T., Deroubaix, A., Darras, S., Elguindi, N., Granier, C., Lacey, F., Müller, J.-F., Shi, X., Tilmes, S., Wang, T., and Basseur, G. P.: Global Changes in Secondary Atmospheric Pollutants During the 2020 COVID-19 Pandemic, *Journal of Geophysical Research: Atmospheres*, 126, e2020JD034213, <https://doi.org/10.1029/2020JD034213>, 2021.
- 650 Gligorovski, S., Grgić, I., Net, S., Böge, O., Inuma, Y., Kahnt, A., Scheinhardt, S., Herrmann, H., and Wortham, H.: Light-induced multiphase chemistry of gas phase ozone on aqueous pyruvic and oxalic acids: Aerosol chamber study, AGU Fall Meeting Abstracts, 2010.
- 655 Herrmann, H.: Kinetics of Aqueous Phase Reactions Relevant for Atmospheric Chemistry, *Chemical Reviews*, 103, 4691-4716, 10.1021/cr020658q, 2003.
- Ho, K. F., Cao, J. J., Lee, S. C., Kawamura, K., Zhang, R. J., Chow, J. C., and Watson, J. G.: Dicarboxylic acids, ketocarboxylic acids, and dicarbonyls in the urban atmosphere of China, *J. Geophys. Res. Atmos.*, 112, D22S27, 10.1029/2006jd008011, 2007.
- 660 Ho, K. F., Ho, S. S. H., Lee, S. C., Kawamura, K., Zou, S. C., Cao, J. J., and Xu, H. M.: Summer and winter variations of dicarboxylic acids, fatty acids and benzoic acid in PM<sub>2.5</sub> in Pearl Delta River Region, China, *Atmos. Chem. Phys.*, 11, 2197-2208, 10.5194/acp-11-2197-2011, 2011.
- Huang, R.-J., Zhang, Y., Bozzetti, C., Ho, K.-F., Cao, J.-J., Han, Y., Daellenbach, K. R., Slowik, J. G., Platt, S. M., Canonaco, F., Zotter, P., Wolf, R., Pieber, S. M., Bruns, E. A., Crippa, M., Ciarelli, G., Piazzalunga, A., Schwikowski, M., Abbaszade, G., Schnelle-Kreis, J., Zimmermann, R., An, Z., Szidat, S., Baltensperger, U., Haddad, I. E., and Prévôt, A. S. H.: High secondary aerosol contribution to particulate pollution during haze events in China, *Nature*, 514, 218, 10.1038/nature13774, <https://www.nature.com/articles/nature13774#supplementary-information>, 2014.
- 665 Huang, X., Ding, A., Gao, J., Zheng, B., Zhou, D., Qi, X., Tang, R., Wang, J., Ren, C., Nie, W., Chi, X., Xu, Z., Chen, L., Li, Y., Che, F., Pang, N., Wang, H., Tong, D., Qin, W., Cheng, W., Liu, W., Fu, Q., Liu, B., Chai, F., Davis, S. J., Zhang, Q., and He, K.: Enhanced secondary pollution offset reduction of primary emissions during COVID-19 lockdown in China, *Natl. Sci. Rev.*, 10.1093/nsr/nwaa137, 2020.
- Jang, M., Czoschke, N. M., Lee, S., and Kamens, R. M.: Heterogeneous Atmospheric Aerosol Production by Acid-Catalyzed Particle-Phase Reactions, *Science*, 298, 814, 2002.
- Jung, J., Tsatsral, B., Kim, Y. J., and Kawamura, K.: Organic and inorganic aerosol compositions in Ulaanbaatar, Mongolia, during the cold winter of 2007 to 2008: Dicarboxylic acids, ketocarboxylic acids, and  $\alpha$ -dicarbonyls, *Journal of Geophysical Research: Atmospheres*, 115, D22203, 10.1029/2010jd014339, 2010.
- 675 Kang, M., Zhang, J., Zhang, H., and Ying, Q.: On the Relevancy of Observed Ozone Increase during COVID-19 Lockdown to Summertime Ozone and PM<sub>2.5</sub> Control Policies in China, *Environmental Science & Technology Letters*, 8, 289-294, 10.1021/acs.estlett.1c00036, 2021.
- 680 Kawamura, K. and Bikkina, S.: A review of dicarboxylic acids and related compounds in atmospheric aerosols: Molecular distributions, sources and transformation, *Atmos. Res.*, 170, 140-160, <http://dx.doi.org/10.1016/j.atmosres.2015.11.018>, 2016.
- Kawamura, K. and Kaplan, I. R.: Motor exhaust emissions as a primary source for dicarboxylic acids in Los Angeles ambient air, *Environ. Sci. Technol.*, 21, 105-110, 10.1021/es00155a014, 1987.
- 685 Kawamura, K. and Usukura, K.: Distributions of low molecular weight dicarboxylic acids in the North Pacific aerosol samples, *J. Oceano.*, 49, 271-283, 10.1007/bf02269565, 1993.
- Kawamura, K. and Watanabe, T.: Determination of Stable Carbon Isotopic Compositions of Low Molecular Weight

Dicarboxylic Acids and Ketocarboxylic Acids in Atmospheric Aerosol and Snow Samples, *Anal. Chem.*, 76, 5762-5768, 10.1021/ac049491m, 2004.

- 690 Kawamura, K. and Yasui, O.: Diurnal changes in the distribution of dicarboxylic acids, ketocarboxylic acids and dicarbonyls in the urban Tokyo atmosphere, *Atmospheric Environment*, 39, 1945-1960, <http://dx.doi.org/10.1016/j.atmosenv.2004.12.014>, 2005.
- Kawamura, K., Tachibana, E., Okuzawa, K., Aggarwal, S. G., Kanaya, Y., and Wang, Z. F.: High abundances of water-soluble dicarboxylic acids, ketocarboxylic acids and  $\alpha$ -dicarbonyls in the mountain aerosols over the North China Plain during wheat burning season, *Atmos. Chem. Phys.*, 13, 3695-3734, 10.5194/acpd-13-3695-2013, 2013.
- Kundu, S., Kawamura, K., Andreae, T. W., Hoffer, A., and Andreae, M. O.: Molecular distributions of dicarboxylic acids, ketocarboxylic acids and  $\alpha$ -dicarbonyls in biomass burning aerosols: implications for photochemical production and degradation in smoke layers, *Atmos. Chem. Phys.*, 10, 2209-2225, 10.5194/acp-10-2209-2010, 2010.
- 700 Kunwar, B., Kawamura, K., Fujiwara, S., Fu, P., Miyazaki, Y., and Pokhrel, A.: Dicarboxylic acids, oxocarboxylic acids and  $\alpha$ -dicarbonyls in atmospheric aerosols from Mt. Fuji, Japan: Implication for primary emission versus secondary formation, *Atmospheric Research*, 221, 58-71, <https://doi.org/10.1016/j.atmosres.2019.01.021>, 2019.
- Le, T., Wang, Y., Liu, L., Yang, J., Yung, Y. L., Li, G., and Seinfeld, J. H.: Unexpected air pollution with marked emission reductions during the COVID-19 outbreak in China, *Science*, eabb7431, 10.1126/science.abb7431, 2020.
- 705 Levy, M., Zhang, R., Zheng, J., Zhang, A. L., Xu, W., Gomez-Hernandez, M., Wang, Y., and Olague, E.: Measurements of nitrous acid (HONO) using ion drift-chemical ionization mass spectrometry during the 2009 SHARP field campaign, *Atmospheric Environment*, 94, 231-240, <https://doi.org/10.1016/j.atmosenv.2014.05.024>, 2014.
- Li, L., Li, Q., Huang, L., Wang, Q., Zhu, A., Xu, J., Liu, Z., Li, H., Shi, L., Li, R., Azari, M., Wang, Y., Zhang, X., Liu, Z., Zhu, Y., Zhang, K., Xue, S., Ooi, M. C. G., Zhang, D., and Chan, A.: Air quality changes during the COVID-19 lockdown over the Yangtze River Delta Region: An insight into the impact of human activity pattern changes on air pollution variation, *Sci. Total Environ.*, 732, 139282, <https://doi.org/10.1016/j.scitotenv.2020.139282>, 2020.
- 710 Li, K., Jacob, D. J., Liao, H., Shen, L., Zhang, Q., and Bates, K. H.: Anthropogenic drivers of 2013–2017 trends in summer surface ozone in China, *Proceedings of the National Academy of Sciences*, 116, 422, 10.1073/pnas.1812168116, 2019.
- 715 Li, X.-d., Yang, Z., Fu, P., Yu, J., Lang, Y.-c., Liu, D., Ono, K., and Kawamura, K.: High abundances of dicarboxylic acids, oxocarboxylic acids, and  $\alpha$ -dicarbonyls in fine aerosols (PM<sub>2.5</sub>) in Chengdu, China during wintertime haze pollution, *Environmental Science and Pollution Research*, 22, 12902-12918, 10.1007/s11356-015-4548-x, 2015.
- Li, Z., Zhou, R., Wang, Y., Wang, G., Chen, M., Li, Y., Wang, Y., Yi, Y., Hou, Z., Guo, Q., and Meng, J.: Characteristics and sources of amine-containing particles in the urban atmosphere of Liaocheng, a seriously polluted city in North China during the COVID-19 outbreak, *Environ. Pollut.*, 289, 117887, <https://doi.org/10.1016/j.envpol.2021.117887>, 2021a.
- 720 Li, Z., Zhou, R., Li, Y., Chen, M., Wang, Y., Huang, T., Yi, Y., Hou, Z., Meng, J., and Yan, L.: Characteristics and Sources of Organic Aerosol Markers in PM<sub>2.5</sub>, *Aerosol and Air Quality Research*, 21, 210180, 10.4209/aaqr.210180, 2021b.
- Lim, Y. B., Tan, Y., and Turpin, B. J.: Chemical insights, explicit chemistry, and yields of secondary organic aerosol from OH radical oxidation of methylglyoxal and glyoxal in the aqueous phase, *Atmos. Chem. Phys.*, 13, 8651-8667, 10.5194/acp-13-8651-2013, 2013.
- 725 Liu, J., Zhou, S., Zhang, Z., Kawamura, K., Zhao, W., Wang, X., Shao, M., Jiang, F., Liu, J., Sun, X., Hang, J., Zhao, J., Pei, C., Zhang, J., and Fu, P.: Characterization of dicarboxylic acids, oxoacids, and  $\alpha$ -dicarbonyls in PM<sub>2.5</sub> within the urban boundary layer in southern China: Sources and formation pathways, *Environ. Pollut.*, 285, 117185, <https://doi.org/10.1016/j.envpol.2021.117185>, 2021.
- 730

- Lu, K., Guo, S., Tan, Z., Wang, H., Shang, D., Liu, Y., Li, X., Wu, Z., Hu, M., and Zhang, Y.: Exploring atmospheric free-radical chemistry in China: the self-cleansing capacity and the formation of secondary air pollution, *National Science Review*, 6, 579-594, 10.1093/nsr/nwy073, 2019.
- 735 Lv, S., Wang, F., Wu, C., Chen, Y., Liu, S., Zhang, S., Li, D., Du, W., Zhang, F., Wang, H., Huang, C., Fu, Q., Duan, Y., and Wang, G.: Gas-to-Aerosol Phase Partitioning of Atmospheric Water-Soluble Organic Compounds at a Rural Site in China: An Enhancing Effect of NH<sub>3</sub> on SOA Formation, *Environ. Sci. Technol.*, 56, 3915-3924, 10.1021/acs.est.1c06855, 2022.
- 740 Meng, J., Liu, X., Hou, Z., Yi, Y., Yan, L., Li, Z., Cao, J., Li, J., and Wang, G.: Molecular characteristics and stable carbon isotope compositions of dicarboxylic acids and related compounds in the urban atmosphere of the North China Plain: Implications for aqueous phase formation of SOA during the haze periods, *Sci. Total Environ.*, 705, 135256, <https://doi.org/10.1016/j.scitotenv.2019.135256>, 2020.
- 745 Meng, J., Li, Z., Zhou, R., Chen, M., Li, Y., Yi, Y., Ding, Z., Li, H., Yan, L., Hou, Z., and Wang, G.: Enhanced photochemical formation of secondary organic aerosols during the COVID-19 lockdown in Northern China, *Sci. Total Environ.*, 758, 143709, <https://doi.org/10.1016/j.scitotenv.2020.143709>, 2021.
- Meng, J., Wang, G., Hou, Z., Liu, X., Wei, B., Wu, C., Cao, C., Wang, J., Li, J., Cao, J., Zhang, E., Dong, J., Liu, J., Ge, S., and Xie, Y.: Molecular distribution and stable carbon isotopic compositions of dicarboxylic acids and related SOA from biogenic sources in the summertime atmosphere of Mt. Tai in the North China Plain, *Atmos. Chem. Phys.*, 18, 15069-15086, 10.5194/acp-18-15069-2018, 2018.
- 750 Meng, J., Wang, G., Li, J., Cheng, C., Ren, Y., Huang, Y., Cheng, Y., Cao, J., and Zhang, T.: Seasonal characteristics of oxalic acid and related SOA in the free troposphere of Mt. Hua, central China: Implications for sources and formation mechanisms, *Science of The Total Environment*, 493, 1088-1097, <http://dx.doi.org/10.1016/j.scitotenv.2014.04.086>, 2014.
- Miyazaki, Y., Aggarwal, S. G., Singh, K., Gupta, P. K., and Kawamura, K.: Dicarboxylic acids and water-soluble organic carbon in aerosols in New Delhi, India, in winter: Characteristics and formation processes, *J. Geophys. Res. Atmos.*, 114, D19206, 10.1029/2009jd011790, 2009.
- 755 Mochizuki, T., Kawamura, K., Miyazaki, Y., Wada, R., Takahashi, Y., Saigusa, N., and Tani, A.: Secondary formation of oxalic acid and related organic species from biogenic sources in a larch forest at the northern slope of Mt. Fuji, *Atmos. Environ.*, 166, 255-262, <https://doi.org/10.1016/j.atmosenv.2017.07.028>, 2017.
- Myriokefalitakis, S., Tsigaridis, K., Mihalopoulos, N., Sciare, J., Nenes, A., Kawamura, K., Segers, A., and Kanakidou, M.: In-cloud oxalate formation in the global troposphere: a 3-D modeling study, *Atmos. Chem. Phys.*, 11, 5761-5782, 10.5194/acp-11-5761-2011, 2011.
- 760 Narukawa, M., Kawamura, K., Takeuchi, N., and Nakajima, T.: Distribution of dicarboxylic acids and carbon isotopic compositions in aerosols from 1997 Indonesian forest fires, *Geophys. Res. Lett.*, 26, 3101-3104, <https://doi.org/10.1029/1999GL010810>, 1999.
- 765 Pavuluri, C. M. and Kawamura, K.: Evidence for <sup>13</sup>C-enrichment in oxalic acid via iron catalyzed photolysis in aqueous phase, *Geophysical Research Letters*, 39, L03802, 10.1029/2011gl050398, 2012.
- Pavuluri, C. M. and Kawamura, K.: Enrichment of <sup>13</sup>C in diacids and related compounds during photochemical processing of aqueous aerosols: New proxy for organic aerosols aging, *Sci. Rep.*, 6, 36467, 10.1038/srep36467, 2016.
- 770 Pavuluri, C. M., Kawamura, K., Tachibana, E., and Swaminathan, T.: Elevated nitrogen isotope ratios of tropical Indian aerosols from Chennai: Implication for the origins of aerosol nitrogen in South and Southeast Asia, *Atmospheric Environment*, 44, 3597-3604, <https://doi.org/10.1016/j.atmosenv.2010.05.039>, 2010.
- Perri, M. J., Seitzinger, S., and Turpin, B. J.: Secondary organic aerosol production from aqueous photooxidation of glycolaldehyde: Laboratory experiments, *Atmospheric Environment*, 43, 1487-1497,

<https://doi.org/10.1016/j.atmosenv.2008.11.037>, 2009.

- 775 Rinaldi, M., Decesari, S., Carbone, C., Finessi, E., Fuzzi, S., Ceburnis, D., O'Dowd, C. D., Sciare, J., Burrows, J. P., Vrekoussis, M., Ervens, B., Tsigaridis, K., and Facchini, M. C.: Evidence of a natural marine source of oxalic acid and a possible link to glyoxal, *J. Geophys. Res. Atmos.*, 116, n/a-n/a, 10.1029/2011jd015659, 2011.
- Shen, M., Ho, K. F., Dai, W., Liu, S., Zhang, T., Wang, Q., Meng, J., Chow, J. C., Watson, J. G., Cao, J., and Li, J.: Distribution and stable carbon isotopic composition of dicarboxylic acids, ketocarboxylic acids and  $\alpha$ -dicarbonyls in fresh and aged biomass burning aerosols, *Atmos. Chem. Phys.*, 22, 7489-7504, 10.5194/acp-22-7489-2022, 2022.
- 780 Shen, M., Qi, W., Guo, X., Dai, W., Wang, Q., Liu, Y., Zhang, Y., Cao, Y., Chen, Y., Li, L., Liu, H., Cao, J., and Li, J.: Influence of vertical transport on chemical evolution of dicarboxylic acids and related secondary organic aerosol from surface emission to the top of Mount Hua, Northwest China, *Science of The Total Environment*, 858, 159892, <https://doi.org/10.1016/j.scitotenv.2022.159892>, 2023.
- 785 Shi, Z., Song, C., Liu, B., Lu, G., Xu, J., Van Vu, T., Elliott Robert, J. R., Li, W., Bloss William, J., and Harrison Roy, M.: Abrupt but smaller than expected changes in surface air quality attributable to COVID-19 lockdowns, *Sci. Adv.*, 7, eabd6696, 10.1126/sciadv.abd6696, 2021.
- Sorathia, F., Rajput, P., and Gupta, T.: Dicarboxylic acids and levoglucosan in aerosols from Indo-Gangetic Plain: Inferences from day night variability during wintertime, *Sci. Total Environ.*, 624, 451-460, <https://doi.org/10.1016/j.scitotenv.2017.12.124>, 2018.
- 790 Surratt, J. D., Lewandowski, M., Offenberg, J. H., Jaoui, M., Kleindienst, T. E., Edney, E. O., and Seinfeld, J. H.: Effect of Acidity on Secondary Organic Aerosol Formation from Isoprene, *Environ. Sci. Technol.*, 41, 5363-5369, 10.1021/es0704176, 2007.
- 795 Tan, Y., Perri, M. J., Seitzinger, S. P., and Turpin, B. J.: Effects of Precursor Concentration and Acidic Sulfate in Aqueous Glyoxal-OH Radical Oxidation and Implications for Secondary Organic Aerosol, *Environmental Science & Technology*, 43, 8105-8112, 10.1021/es901742f, 2009.
- Wang, G., Cheng, C., Meng, J., Huang, Y., Li, J., and Ren, Y.: Field observation on secondary organic aerosols during Asian dust storm periods: Formation mechanism of oxalic acid and related compounds on dust surface, *Atmos. Environ.*, 800 113, 169-176, <http://dx.doi.org/10.1016/j.atmosenv.2015.05.013>, 2015.
- Wang, G., Xie, M., Hu, S., Gao, S., Tachibana, E., and Kawamura, K.: Dicarboxylic acids, metals and isotopic compositions of C and N in atmospheric aerosols from inland China: implications for dust and coal burning emission and secondary aerosol formation, *Atmos. Chem. Phys.*, 10, 6087-6096, 10.5194/acp-10-6087-2010, 2010.
- Wang, G., Kawamura, K., Cheng, C., Li, J., Cao, J., Zhang, R., Zhang, T., Liu, S., and Zhao, Z.: Molecular Distribution and Stable Carbon Isotopic Composition of Dicarboxylic Acids, Ketocarboxylic Acids, and  $\alpha$ -Dicarbonyls in Size-Resolved Atmospheric Particles From Xi 'an City, China, *Environ. Sci. Technol.*, 46, 4783-4791, 805 10.1021/es204322c, 2012.
- Wang, G., Zhang, R., Gomez, M. E., Yang, L., Levy Zamora, M., Hu, M., Lin, Y., Peng, J., Guo, S., Meng, J., Li, J., Cheng, C., Hu, T., Ren, Y., Wang, Y., Gao, J., Cao, J., An, Z., Zhou, W., Li, G., Wang, J., Tian, P., Marrero-Ortiz, W., 810 Secrest, J., Du, Z., Zheng, J., Shang, D., Zeng, L., Shao, M., Wang, W., Huang, Y., Wang, Y., Zhu, Y., Li, Y., Hu, J., Pan, B., Cai, L., Cheng, Y., Ji, Y., Zhang, F., Rosenfeld, D., Liss, P. S., Duce, R. A., Kolb, C. E., and Molina, M. J.: Persistent sulfate formation from London Fog to Chinese haze, *P. Natl. Acad. Sci. USA*, 113, 13630-13635, 10.1073/pnas.1616540113, 2016.
- Wang, H. and Kawamura, K.: Stable carbon isotopic composition of low-molecular-weight dicarboxylic acids and ketoacids in remote marine aerosols, *J. Geophys. Res. Atmos.*, 111, <https://doi.org/10.1029/2005JD006466>, 2006.
- 815 Wang, J., Wang, G., Gao, J., Wang, H., Ren, Y., Li, J., Zhou, B., Wu, C., Zhang, L., Wang, S., and Chai, F.: Concentrations

and stable carbon isotope compositions of oxalic acid and related SOA in Beijing before, during, and after the 2014 APEC, *Atmos. Chem. Phys.*, 17, 981-992, 10.5194/acp-17-981-2017, 2017.

820 Wang, J., Wang, G., Wu, C., Li, J., Cao, C., Li, J., Xie, Y., Ge, S., Chen, J., Zeng, L., Zhu, T., Zhang, R., and Kawamura, K.: Enhanced aqueous-phase formation of secondary organic aerosols due to the regional biomass burning over North China Plain, *Environ. Pollut.*, 256, 113401, <https://doi.org/10.1016/j.envpol.2019.113401>, 2020a.

825 Wang, N., Xu, J., Pei, C., Tang, R., Zhou, D., Chen, Y., Li, M., Deng, X., Deng, T., Huang, X., and Ding, A.: Air Quality During COVID-19 Lockdown in the Yangtze River Delta and the Pearl River Delta: Two Different Responsive Mechanisms to Emission Reductions in China, *Environmental Science & Technology*, 55, 5721-5730, 10.1021/acs.est.0c08383, 2021.

Wang, P., Chen, K., Zhu, S., Wang, P., and Zhang, H.: Severe air pollution events not avoided by reduced anthropogenic activities during COVID-19 outbreak, *Resour. Conserv. Recy.*, 158, 104814, <https://doi.org/10.1016/j.resconrec.2020.104814>, 2020b.

830 Warneck, P.: In-cloud chemistry opens pathway to the formation of oxalic acid in the marine atmosphere, *Atmos. Environ.*, 37, 2423-2427, [http://dx.doi.org/10.1016/S1352-2310\(03\)00136-5](http://dx.doi.org/10.1016/S1352-2310(03)00136-5), 2003.

Weller, C., Tilgner, A., Bräuer, P., and Herrmann, H.: Modeling the Impact of Iron–Carboxylate Photochemistry on Radical Budget and Carboxylate Degradation in Cloud Droplets and Particles, *Environmental Science & Technology*, 48, 5652-5659, 10.1021/es4056643, 2014.

835 Wu, J., Bei, N., Hu, B., Liu, S., Wang, Y., Shen, Z., Li, X., Liu, L., Wang, R., Liu, Z., Cao, J., Tie, X., Molina, L. T., and Li, G.: Aerosol–photolysis interaction reduces particulate matter during wintertime haze events, *P. Natl. Acad. Sci. USA*, 117, 9755-9761, 10.1073/pnas.1916775117, 2020.

840 Xu, B., Zhang, G., Gustafsson, Ö., Kawamura, K., Li, J., Andersson, A., Bikkina, S., Kunwar, B., Pokhrel, A., Zhong, G., Zhao, S., Li, J., Huang, C., Cheng, Z., Zhu, S., Peng, P., and Sheng, G.: Large contribution of fossil-derived components to aqueous secondary organic aerosols in China, *Nat. Commun.*, 13, 5115, 10.1038/s41467-022-32863-3, 2022.

Xu, K., Cui, K., Young, L.-H., Wang, Y.-F., Hsieh, Y.-K., Wan, S., and Zhang, J.: Air Quality Index, Indicator Air Pollutants and Impact of COVID-19 Event on the Air Quality near Central China, *Aerosol and Air Quality Research*, 20, 1204-1221, 10.4209/aaqr.2020.04.0139, 2020.

845 Yu, J. Z., Huang, X.-F., Xu, J., and Hu, M.: When Aerosol Sulfate Goes Up, So Does Oxalate: Implication for the Formation Mechanisms of Oxalate, *Environmental Science & Technology*, 39, 128-133, 10.1021/es049559f, 2005.

Yu, Q., Chen, J., Cheng, S., Qin, W., Zhang, Y., Sun, Y., and Ahmad, M.: Seasonal variation of dicarboxylic acids in PM<sub>2.5</sub> in Beijing: Implications for the formation and aging processes of secondary organic aerosols, *Sci. Total Environ.*, 763, 142964, <https://doi.org/10.1016/j.scitotenv.2020.142964>, 2021.

850 Yu, Q., Chen, J., Qin, W., Cheng, S., Zhang, Y., Ahmad, M., and Ouyang, W.: Characteristics and secondary formation of water-soluble organic acids in PM<sub>1</sub>, PM<sub>2.5</sub> and PM<sub>10</sub> in Beijing during haze episodes, *Sci. Total Environ.*, 669, 175-184, <https://doi.org/10.1016/j.scitotenv.2019.03.131>, 2019.

Zhang, Y., Kawamura, K., Cao, F., and Lee, M.: Stable carbon isotopic compositions of low-molecular-weight dicarboxylic acids, oxocarboxylic acids,  $\alpha$ -dicarbonyls, and fatty acids: Implications for atmospheric processing of organic aerosols, *J. Geophys. Res. Atmos.*, 121, 3707-3717, 10.1002/2015jd024081, 2016.

855 Zhao, W., Kawamura, K., Yue, S., Wei, L., Ren, H., Yan, Y., Kang, M., Li, L., Ren, L., Lai, S., Li, J., Sun, Y., Wang, Z., and Fu, P.: Molecular distribution and compound-specific stable carbon isotopic composition of dicarboxylic acids, oxocarboxylic acids and  $\alpha$ -dicarbonyls in PM<sub>2.5</sub> from Beijing, China, *Atmos. Chem. Phys.*, 18, 2749-2767, 10.5194/acp-18-2749-2018, 2018.

Zhao, W., Ren, H., Kawamura, K., Du, H., Chen, X., Yue, S., Xie, Q., Wei, L., Li, P., Zeng, X., Kong, S., Sun, Y., Wang, Z.,

- 860 and Fu, P.: Vertical distribution of particle-phase dicarboxylic acids, oxoacids and  $\alpha$ -dicarbonyls in the urban boundary layer based on the 325 m tower in Beijing, *Atmos. Chem. Phys.*, 20, 10331-10350, 10.5194/acp-20-10331-2020, 2020.
- 865 Zhao, X., Pavuluri, C. M., Dong, Z., Xu, Z., Nirmalkar, J., Jung, J., Fu, P., and Liu, C.-Q.: Molecular Distributions and  $^{13}\text{C}$  Isotopic Composition of Dicarboxylic Acids, Oxocarboxylic Acids, and  $\alpha$ -dicarbonyls in Wintertime PM<sub>2.5</sub> at Three Sites Over Northeast Asia: Implications for Origins and Long-Range Atmospheric Transport, *Journal of Geophysical Research: Atmospheres*, 128, e2023JD038864, <https://doi.org/10.1029/2023JD038864>, 2023.
- Zhong, H., Huang, R., Chang, Y., Duan, J., Lin, C., and Chen, Y.: Enhanced formation of secondary organic aerosol from photochemical oxidation during the COVID-19 lockdown in a background site in Northwest China, *Sci. Total Environ.*, 778, 144947, <https://doi.org/10.1016/j.scitotenv.2021.144947>, 2021.
- 870 Zhou, Y., Huang, X. H., Bian, Q., Griffith, S. M., Louie, P. K. K., and Yu, J. Z.: Sources and atmospheric processes impacting oxalate at a suburban coastal site in Hong Kong: Insights inferred from 1 year hourly measurements, *Journal of Geophysical Research: Atmospheres*, 120, 9772-9788, <https://doi.org/10.1002/2015JD023531>, 2015.

## Table captions

875

Table 1. Meteorological parameters, liquid water content (LWC) of aerosol, in-situ pH ( $\text{pH}_{\text{is}}$ ), and chemical compositions of  $\text{PM}_{2.5}$  before (January 6 – 23, 2020) and during the lockdown (LCD) (January 31 – February 17, 2020) in Jinan, China.

880

Table 2. Concentrations ( $\text{ng m}^{-3}$ ) of dicarboxylic acids, oxocarboxylic acids, and  $\alpha$ -dicarbonyls in  $\text{PM}_{2.5}$  before and during the LCD in Jinan, China.

Table 3. Differences in the stable carbon isotopic compositions ( $\delta^{13}\text{C}$ , ‰) of major detected diacids and related compounds before and during the LCD in Jinan, China.

885

## Figure captions

Figure 1. Temporal variations of gaseous pollutants, meteorological parameters, and chemical compositions of  $\text{PM}_{2.5}$  before and during the LCD in Jinan, China.

890

Figure 2. Correlation analysis between the ratio of the total concentration of detected organic components (TDOCs) normalized by CO (TDOCs/CO) and temperature, and between diacids and oxoacids (a) and (b) before the LCD, (c) and (d) during the LCD in Jinan, China.

895

Figure 3. Diurnal changes of (a) major organic compounds and (b) selected mass ratios before and during the LCD in Jinan, China (<sup>a</sup> the concentrations reduced by 10 times; <sup>b</sup> TDOCs: total detected organic components; <sup>c</sup> the mass ratios enlarged by 5 times; <sup>d</sup> the mass ratio enlarged by 100 times).

900

Figure 4. Correlation coefficients ( $R^2$ ) of concentrations of  $\text{C}_2$  and its organic precursors and selected ratios with influencing factors (a) before the LCD and (b) during the LCD in Jinan, China.

Figure 5. Temporal variations in the concentrations of levoglucosan, diacids,  $\text{C}_2$  and its major precursors, the ratios of  $\text{C}_2/\text{Diacids}$ , as well as liquid water content (LWC), in-situ pH ( $\text{pH}_{\text{is}}$ ), temperature, relative humidity (RH), solar radiation, and  $\text{O}_3$  before and during the LCD in Jinan, China.

905

Figure 6. Differences in the stable carbon isotope compositions of major detected diacids ( $\text{C}_2\text{--C}_4$ , tPh), the smallest oxoacids ( $\omega\text{C}_2$ ), and  $\alpha$ -dicarbonyls including Gly and mGly before and during the LCD in the atmosphere of Jinan, China.

910

Figure 7. Comparison of stable carbon isotopic compositions ( $\delta^{13}\text{C}$ , ‰) of  $\text{C}_2$  in aerosols of Jinan with those in other regions in the winter.

Figure 8. Correlations of the  $\delta^{13}\text{C}$  of  $\text{C}_2$  with the mass ratios of  $\text{C}_2/\text{Gly}$ ,  $\text{C}_2/\text{mGly}$ ,  $\text{C}_2/\text{Diacids}$ ,  $\text{C}_2/\omega\text{C}_2$ , and  $\text{C}_2/\text{kC}_3$ , and the  $\delta^{13}\text{C}$  of tPh with the mass ratio of tPh/Diacids before and during the LCD in January to February 2020.

915

Figure 9. Source profiles of major chemical components in the  $\text{PM}_{2.5}$  samples from Jinan (a, c) before the LCD and (b, d) during the LCD (BB: biomass burning).

Figure 10. Schematic diagram illustrating the sources and formation mechanisms of  $\text{C}_2$  and diacids before and during the LCD.

**Table 1. Meteorological parameters, liquid water content (LWC) of aerosol, in-situ pH (pH<sub>is</sub>), and chemical compositions of PM<sub>2.5</sub> before (January 6 – 23, 2020) and during the lockdown (LCD) (January 31 – February 17, 2020) in Jinan, China.**

|   | Before the LCD ( <i>n</i> =36) | During the LCD ( <i>n</i> =36) | Whole period ( <i>n</i> =72) |
|---|--------------------------------|--------------------------------|------------------------------|
| <b>I. Meteorological parameters</b>                 |                                |                                |                              |
| Temperature (°C)                                    | 0.07 ± 5.9 (-16–13)            | 6.8 ± 5.2 (-3.4–16)            | 3.4 ± 6.5 (-16–16)           |
| Relative humidity (%)                               | 52 ± 10 (30–87)                | 39 ± 18 (17–85)                | 45 ± 16 (17–87)              |
| Solar radiation (W m <sup>-2</sup> )                | 164 ± 70 (32–282)              | 255 ± 117 (18–423)             | 209 ± 106 (18–423)           |
| Wind speed (m s <sup>-1</sup> )                     | 3.0 ± 0.7 (1.6–4.6)            | 3.7 ± 1.1 (1.2–6.6)            | 3.3 ± 1.0 (1.2–6.6)          |
| <b>II. Gaseous pollutants (µg m<sup>-3</sup>)</b>   |                                |                                |                              |
| SO <sub>2</sub>                                     | 23 ± 8.9 (8.3–49)              | 14 ± 4.9 (4.9–29)              | 18 ± 8.5 (4.9–49)            |
| NO <sub>2</sub>                                     | 56 ± 12 (38–82)                | 21 ± 5.9 (9.3–34)              | 38 ± 20 (9.3–81)             |
| CO  | 1.6 ± 0.3 (0.9–2.5)            | 0.9 ± 0.2 (0.5–1.6)            | 1.3 ± 0.5 (0.5–2.5)          |
| O <sub>3</sub>                                      | 29 ± 18 (5.3–74)               | 66 ± 21 (25–109)               | 48 ± 27 (5.3–109)            |
| OH·radicals (×10 <sup>6</sup> cm <sup>-3</sup> )    | 9.7 ± 9.1 (0.2–21)             | 14 ± 15 (0.3–34)               | 12 ± 12 (0.2–34)             |
| <b>III. Inorganic ions (µg m<sup>-3</sup>)</b>      |                                |                                |                              |
| K <sup>+</sup>                                      | 1.0 ± 0.1 (0.9–1.7)            | 1.3 ± 0.6 (0.5–2.9)            | 1.1 ± 0.4 (0.5–2.9)          |
| Na <sup>+</sup>                                     | 0.3 ± 0.1 (0.1–0.6)            | 0.2 ± 0.1 (0.1–0.8)            | 0.2 ± 0.1 (0.1–0.8)          |
| Ca <sup>2+</sup>                                    | 0.4 ± 0.2 (0.1–0.9)            | 0.5 ± 0.2 (0.2–1.1)            | 0.5 ± 0.2 (0.1–1.1)          |
| Mg <sup>2+</sup>                                    | 0.1 ± 0.03 (0–0.1)             | 0.1 ± 0.1 (0.1–0.4)            | 0.1 ± 0.1 (0–0.4)            |
| NH <sub>4</sub> <sup>+</sup>                        | 11 ± 5.7 (4.4–26)              | 7.7 ± 4.7 (0.4–16)             | 9.6 ± 5.5 (0.4–26)           |
| NO <sub>3</sub> <sup>-</sup>                        | 19 ± 11 (5.4–49)               | 9.6 ± 4.9 (1.2–18)             | 14 ± 9.7 (1.2–49)            |
| SO <sub>4</sub> <sup>2-</sup>                       | 13 ± 6.9 (3.8–31)              | 9.4 ± 5.3 (1.1–18)             | 11 ± 6.4 (1.1–31)            |
| SNA <sup>a</sup>                                    | 44 ± 23 (15–105)               | 27 ± 15 (2.8–50)               | 35 ± 21 (2.8–105)            |
| Subtotal  | 49 ± 24 (18–113)               | 35 ± 18 (6.1–67)               | 42 ± 22 (6.1–113)            |
| <b>IV. Carbonaceous species (µg m<sup>-3</sup>)</b> |                                |                                |                              |
| EC  | 4.3 ± 2.4 (0.9–11)             | 1.9 ± 1.0 (0.3–3.8)            | 3.1 ± 2.2 (0.3–11)           |
| OC  | 10 ± 3.0 (5.2–19)              | 6.4 ± 2.6 (2.0–11)             | 8.3 ± 3.4 (2.0–19)           |
| WSOC  | 3.9 ± 1.9 (1.2–10)             | 3.2 ± 1.4 (1.0–7.0)            | 3.5 ± 1.7 (1.0–10)           |
| OC/EC   | 2.9 ± 1.3 (1.5–6.9)            | 4.0 ± 1.5 (2.4–8.4)            | 3.5 ± 1.5 (1.5–8.4)          |
| WSOC/OC   | 0.4 ± 0.1 (0.2–0.7)            | 0.5 ± 0.1 (0.3–0.8)            | 0.4 ± 0.1 (0.2–0.8)          |
| <b>V. Other species</b>                             |                                |                                |                              |
| PM <sub>2.5</sub> (µg m <sup>-3</sup> )             | 106 ± 45 (35–202)              | 56 ± 29 (10–111)               | 81 ± 46 (10–202)             |
| PM <sub>10</sub> (µg m <sup>-3</sup> )              | 147 ± 58 (38–285)              | 72 ± 33 (19–129)               | 109 ± 60 (19–285)            |
| Levogluconan (ng m <sup>-3</sup> )                  | 141 ± 70 (50–370)              | 102 ± 29 (61–186)              | 121 ± 57 (50–370)            |
| pH <sub>is</sub>                                    | 3.2 ± 3.0 (2.3–7.7)            | 3.5 ± 3.5 (2.8–4.9)            | 3.3 ± 3.1 (2.3–7.7)          |
| LWC (µg m <sup>-3</sup> )                           | 35 ± 33 (4.3–172)              | 10 ± 10 (0.2–45)               | 24 ± 30 (0.2–172)            |
| SNA/PM <sub>2.5</sub> (%)                           | 40 ± 6.5 (29–54)               | 47 ± 8.2 (28–60)               | 43 ± 8.1 (28–60)             |
| N/S <sup>b</sup>                                    | 1.5 ± 0.3 (0.9–2.4)            | 1.1 ± 0.2 (0.7–1.5)            | 1.3 ± 0.4 (0.7–2.4)          |

<sup>a</sup>Total concentration of SO<sub>4</sub><sup>2-</sup>, NO<sub>3</sub><sup>-</sup>, and NH<sub>4</sub><sup>+</sup>.<sup>b</sup>The ratio of NO<sub>3</sub><sup>-</sup>/SO<sub>4</sub><sup>2-</sup>.



**Table 2. Concentrations (ng m<sup>-3</sup>) of dicarboxylic acids, oxocarboxylic acids, and  $\alpha$ -dicarbonyls in PM<sub>2.5</sub> before and during the LCD in Jinan, China.**

| Compounds                                   | Before the LCD ( <i>n</i> = 36) | During the LCD ( <i>n</i> = 36) | Whole period ( <i>n</i> = 72) |
|---|---------------------------------|---------------------------------|-------------------------------|
| <b>I. Dicarboxylic acids</b>                |                                 |                                 |                               |
| Oxalic, C <sub>2</sub>                      | 181 ± 48 (110–381)              | 239 ± 108 (46–478)              | 210 ± 88 (46–478)             |
| Malonic, C <sub>3</sub>                     | 15 ± 4.3 (5.2–26)               | 45 ± 14 (18–79)                 | 30 ± 19 (5.2–79)              |
| Succinic, C <sub>4</sub>                    | 54 ± 29 (15–178)                | 30 ± 13 (11–66)                 | 42 ± 25 (11–178)              |
| Glutaric, C <sub>5</sub>                    | 6.7 ± 4.5 (0.6–20)              | 7.5 ± 4.0 (0.7–15)              | 7.1 ± 4.2 (0.6–20)            |
| Adipic, C <sub>6</sub>                      | 9.2 ± 8.6 (1.7–41)              | 6.1 ± 3.3 (0.9–14)              | 7.6 ± 6.7 (0.9–41)            |
| Pimelic, C <sub>7</sub>                     | 2.3 ± 1.5 (0.2–7.4)             | 1.9 ± 1.4 (0–5.1)               | 2.1 ± 1.5 (0–7.4)             |
| Suberic, C <sub>8</sub>                     | 7.7 ± 4.7 (1.9–23)              | 3.0 ± 2.4 (0.1–13)              | 5.4 ± 4.4 (0.1–23)            |
| Azelaic, C <sub>9</sub>                     | 12 ± 4.0 (5.8–24)               | 5.9 ± 4.8 (0.4–23)              | 9.0 ± 5.3 (0.4–24)            |
| Sebacic, C <sub>10</sub>                    | 3.9 ± 2.3 (1.3–9.9)             | 2.6 ± 1.5 (0.2– 5.1)            | 3.3 ± 2.0 (0.2– 9.9)          |
| Undecanedioic, C <sub>11</sub>              | 4.0 ± 2.9 (0.5–15)              | 3.5 ± 1.9 (0.3–8.6)             | 3.8 ± 2.4 (0.3–15)            |
| Methylmalonic, iC <sub>4</sub>              | 3.5 ± 4.1 (0.2–13)              | 4.8 ± 4.6 (0–17)                | 4.1 ± 4.4 (0–17)              |
| Methylsuccinic, iC <sub>5</sub>             | 4.2 ± 3.5 (0.4–12)              | 3.4 ± 1.6 (0.4–6.1)             | 3.8 ± 2.7 (0.4–12)            |
| Methylglutaric, iC <sub>6</sub>             | 2.2 ± 1.1 (0.4–5.6)             | 2.4 ± 1.4 (0–6.6)               | 2.3 ± 1.3 (0–6.6)             |
| Maleic, M                                   | 6.9 ± 6.2 (0.8–34)              | 5.0 ± 2.3 (0.6–11.0)            | 5.9 ± 4.7 (0.6–34)            |
| Fumaric, F                                  | 10 ± 7.6 (2.3–44)               | 1.5 ± 0.9 (0.2–4.8)             | 5.8 ± 6.9 (0.2–44)            |
| Methylmaleic, mM                            | 5.5 ± 4.3 (1.4–22)              | 4.2 ± 3.3 (0–16)                | 4.9 ± 3.9 (0–22)              |
| Phthalic, Ph                                | 11 ± 6.1 (2.9–34)               | 8.8 ± 6.1 (1.2–25)              | 9.9 ± 6.2 (1.2–34)            |
| Isophthalic, iPh                            | 3.0 ± 3.9 (0.2–24)              | 1.8 ± 2.4 (0–9.9)               | 2.4 ± 3.3 (0–24)              |
| Terephthalic, tPh                           | 2.0 ± 1.4 (0.2–7.5)             | 1.3 ± 0.8 (0.1–2.6)             | 1.6 ± 1.2 (0.1–7.5)           |
| Ketomalonic, kC <sub>3</sub>                | 2.1 ± 1.4 (0.3–6.3)             | 3.0 ± 1.7 (0.2–7.4)             | 2.6 ± 1.6 (0.2–7.4)           |
| Ketopimelic, kC <sub>7</sub>                | 5.1 ± 4.7 (0.8–20)              | 5.7 ± 4.2 (0.2–17)              | 5.4 ± 4.4 (0.2–20)            |
| Subtotal                                    | 351 ± 92 (212–672)              | 386 ± 127 (121–707)             | 369 ± 112 (121–707)           |
| <b>II. Oxocarboxylic acids</b>              |                                 |                                 |                               |
| Pyruvic, Pyr                                | 13 ± 4.9 (4.4–25)               | 21 ± 8.8 (7.3–43)               | 17 ± 8.2 (4.4–43)             |
| Glyoxylic, ωC <sub>2</sub>                  | 24 ± 9.1 (6.6–43)               | 29 ± 8.5 (10–43)                | 26 ± 9.0 (6.6–43)             |
| 3-Oxopropanoic, ωC <sub>3</sub>             | 4.5 ± 4.6 (0.8–25)              | 12 ± 6.5 (0.6–27)               | 8.4 ± 6.9 (0.6–27)            |
| 4-Oxobutanoic, ωC <sub>4</sub>              | 7.1 ± 6.4 (0.8–38)              | 3.1 ± 2.7 (0–12)                | 5.1 ± 5.3 (0–38)              |
| 7-Oxoheptanoic, ωC <sub>7</sub>             | 2.3 ± 2.2 (0.2–8.6)             | 1.9 ± 2.0 (0–8.6)               | 2.1 ± 2.1 (0–8.6)             |
| 8-Oxooctanoic, ωC <sub>8</sub>              | 3.2 ± 2.8 (0.4–16)              | 3.7 ± 2.1 (0.1–9.3)             | 3.4 ± 2.4 (0.1–16)            |
| 9-Oxononanoic, ωC <sub>9</sub>              | 6.9 ± 3.0 (1.5–15)              | 3.4 ± 2.9 (0–9.0)               | 5.2 ± 3.4 (0–15)              |
| Subtotal                                    | 61 ± 20 (25–106)                | 75 ± 17 (37–104)                | 68 ± 19 (25–106)              |
| <b>III. <math>\alpha</math>-Dicarbonyls</b> |                                 |                                 |                               |
| Glyoxal, Gly                                | 13 ± 6.3 (4.4–32)               | 13 ± 5.3 (2.0–28)               | 13 ± 5.8 (2.0–32)             |
| Methylglyoxal, mGly                         | 12 ± 7.6 (2.6–30)               | 12 ± 4.8 (2.4–21)               | 12 ± 6.0 (2.4–30)             |
| Subtotal                                    | 25 ± 14 (7.8–62)                | 25 ± 10 (4.4–49)                | 25 ± 12 (4.4–62)              |
| Total detected species                      | 437 ± 117 (246–833)             | 486 ± 144 (179–825)             | 461 ± 132 (179–833)           |

**Table 3. Differences in the stable carbon isotopic compositions ( $\delta^{13}\text{C}$ , ‰) of major detected diacids and related compounds before and during the LCD in Jinan, China.**

| Compounds                                   | Before the LCD ( $n = 36$ ) | During the LCD ( $n = 36$ ) | Whole period ( $n = 72$ )  |
|---|-----------------------------|-----------------------------|----------------------------|
| <b>I. Dicarboxylic acids</b>                |                             |                             |                            |
| C <sub>2</sub>                              | $-22 \pm 1.9$ (-26 to -17)  | $-19 \pm 2.5$ (-24 to -14)  | $-20 \pm 2.5$ (-26 to -14) |
| C <sub>3</sub>                              | $-25 \pm 4.2$ (-36 to -19)  | $-23 \pm 2.2$ (-26 to -18)  | $-24 \pm 3.6$ (-36 to -18) |
| C <sub>4</sub>                              | $-28 \pm 4.6$ (-39 to -22)  | $-25 \pm 2.4$ (-29 to -20)  | $-26 \pm 4.0$ (-39 to -20) |
| C <sub>6</sub>                              | $-29 \pm 3.4$ (-38 to -23)  | $-27 \pm 2.8$ (-31 to -22)  | $-28 \pm 3.3$ (-38 to -22) |
| C <sub>9</sub>                              | $-27 \pm 1.2$ (-30 to -25)  | $-27 \pm 2.3$ (-32 to -24)  | $-27 \pm 1.8$ (-32 to -24) |
| Ph  | $-39 \pm 6.4$ (-51 to -27)  | $-30 \pm 2.6$ (-36 to -26)  | $-34 \pm 6.4$ (-51 to -26) |
| tPh   | $-37 \pm 4.1$ (-46 to -26)  | $-34 \pm 0.9$ (-36 to -32)  | $-35 \pm 3.1$ (-46 to -26) |
| <b>II. Oxocarboxylic acids</b>              |                             |                             |                            |
| Pyr   | $-28 \pm 4.0$ (-39 to -22)  | $-24 \pm 2.3$ (-29 to -20)  | $-26 \pm 3.9$ (-39 to -20) |
| $\omega\text{C}_2$                          | $-27 \pm 3.6$ (-38 to -22)  | $-23 \pm 2.2$ (-26 to -19)  | $-25 \pm 3.6$ (-38 to -19) |
| $\omega\text{C}_3$                          | $-29 \pm 4.0$ (-40 to -24)  | $-26 \pm 2.3$ (-30 to -22)  | $-28 \pm 3.7$ (-40 to -22) |
| <b>III. <math>\alpha</math>-Dicarbonyls</b> |                             |                             |                            |
| Gly   | $-23 \pm 3.7$ (-36 to -19)  | $-20 \pm 2.2$ (-24 to -16)  | $-21 \pm 3.5$ (-36 to -16) |
| mGly  | $-25 \pm 3.8$ (-37 to -21)  | $-21 \pm 2.0$ (-25 to -18)  | $-23 \pm 3.6$ (-37 to -18) |

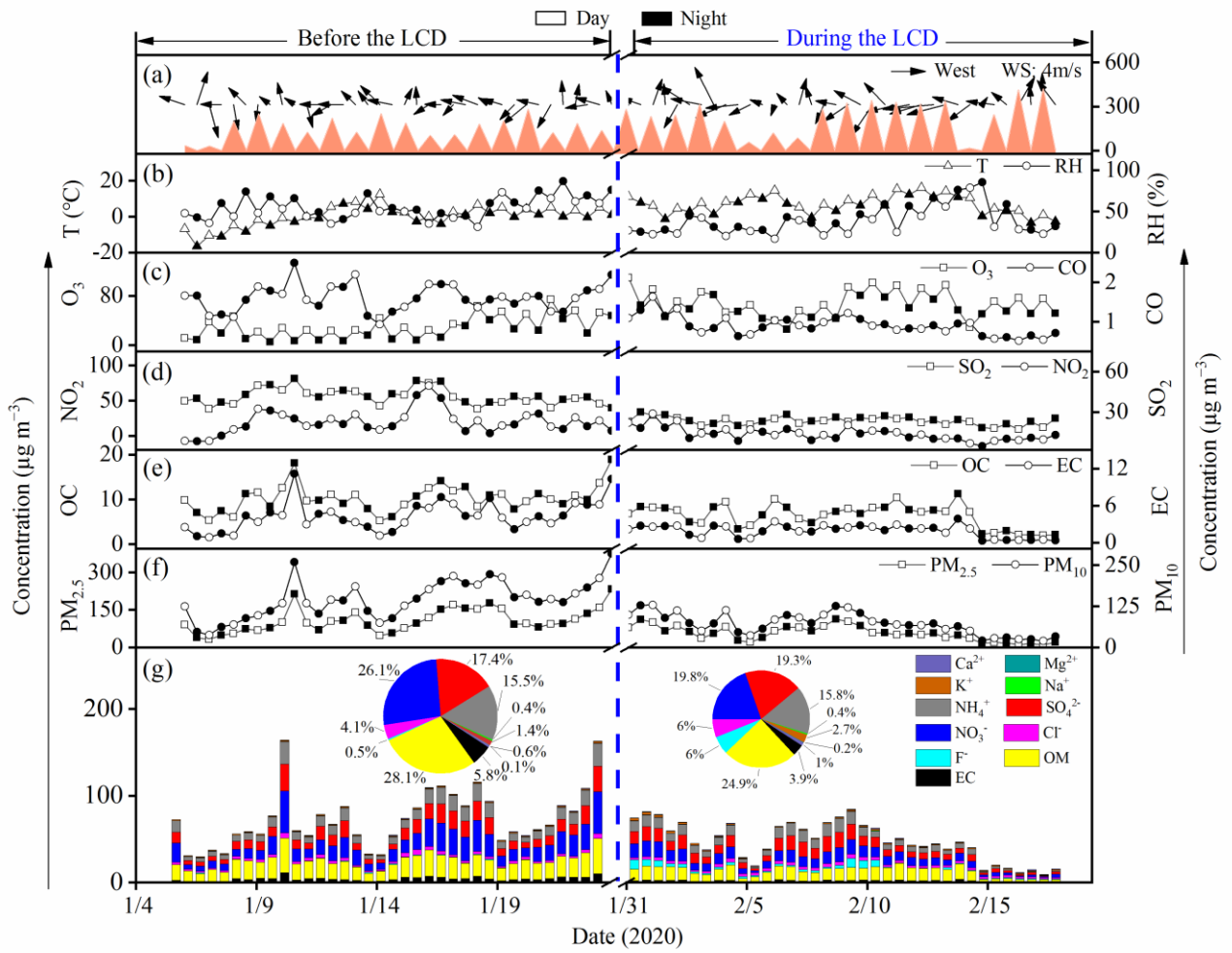
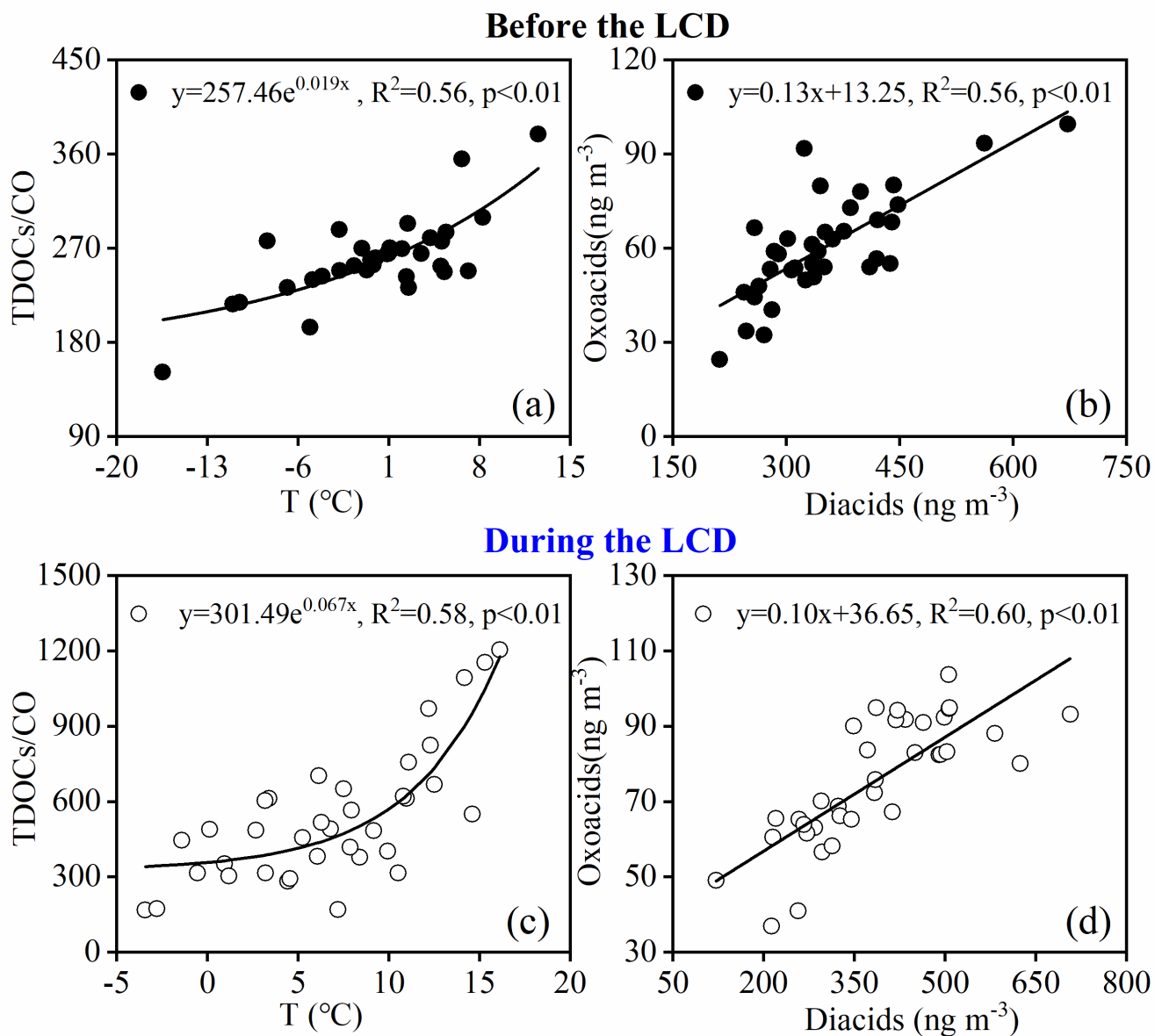


Figure 1. Temporal variations of gaseous pollutants, meteorological parameters, and chemical compositions of PM<sub>2.5</sub> before and during the LCD in Jinan, China.



**Figure 2.** Correlation analysis between the ratio of the total concentration of detected organic components (TDOCs) normalized by CO (TDOCs/CO) and temperature, and between diacids and oxoacids (a) and (b) before the LCD, (c) and (d) during the LCD in Jinan, China.

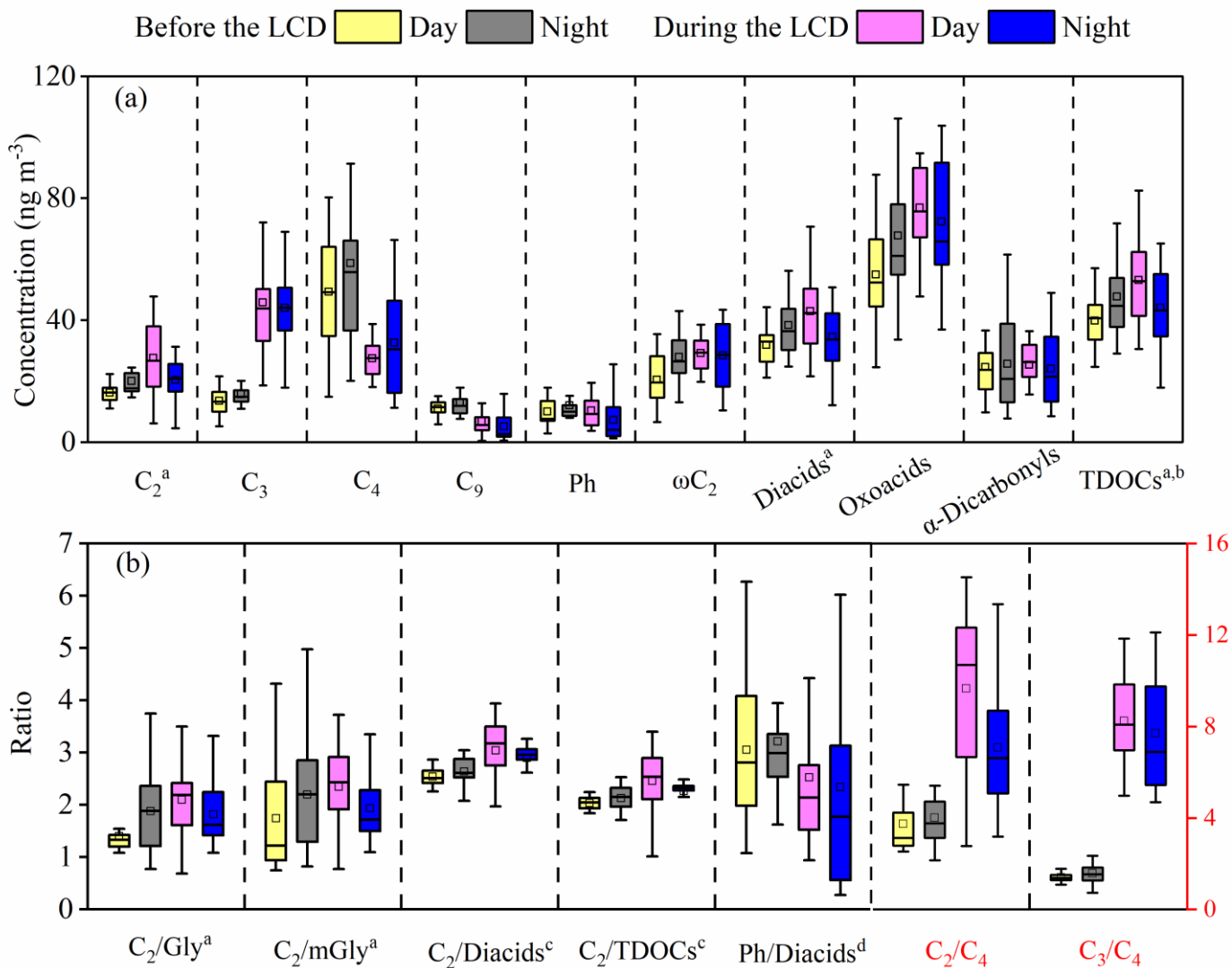
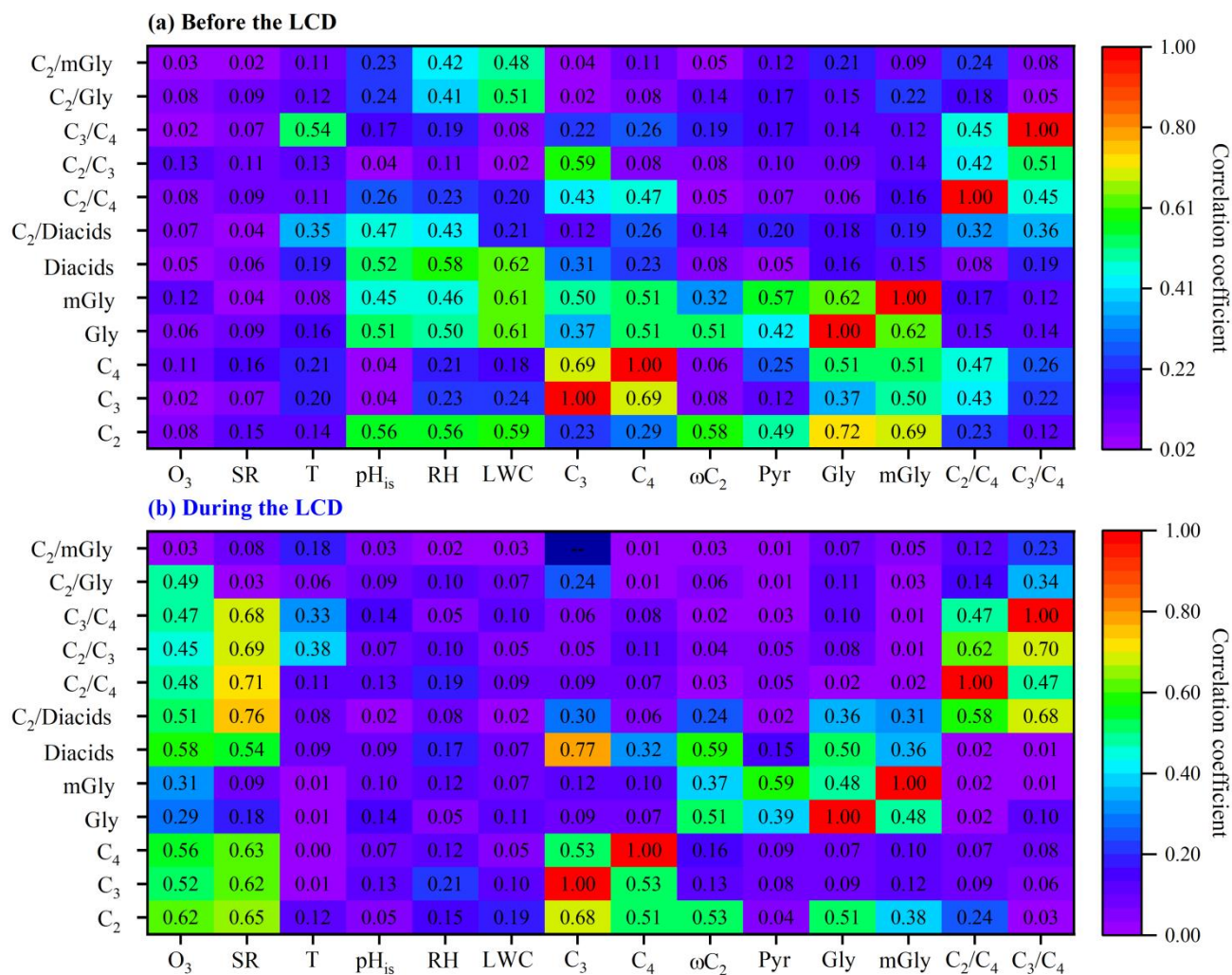
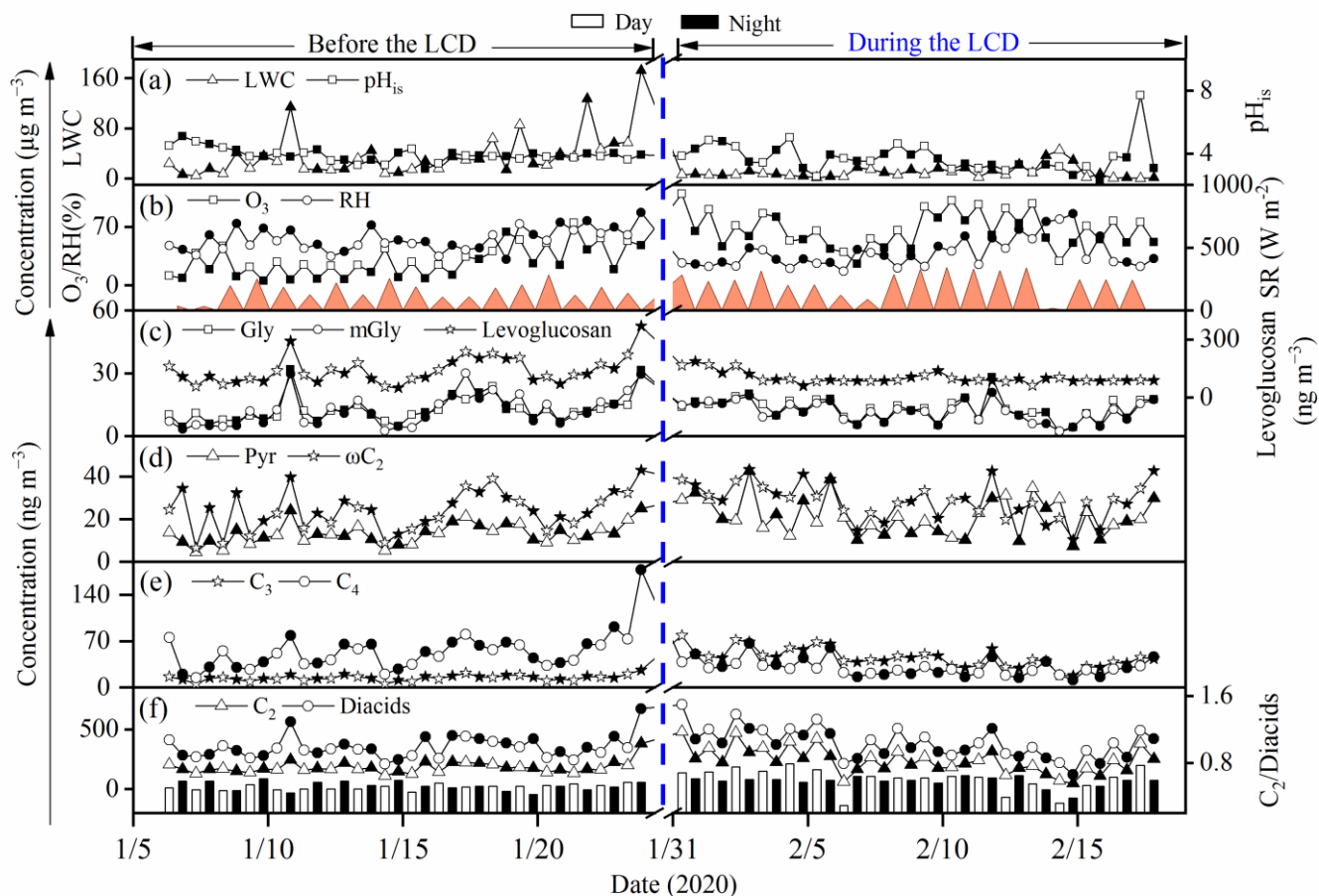


Figure 3. Diurnal changes of (a) major organic compounds and (b) selected mass ratios before and during the LCD in Jinan, China (<sup>a</sup> the concentrations reduced by 10 times; <sup>b</sup> TDOCs: total detected organic components; <sup>c</sup> the mass ratios enlarged by 5 times; <sup>d</sup> the mass ratio enlarged by 100 times).



**Figure 4.** Correlation coefficients ( $R^2$ ) of concentrations of  $C_2$  and its organic precursors and selected ratios with influencing factors (a) before the LCD and (b) during the LCD in Jinan, China.



950

**Figure 5.** Temporal variations in the concentrations of levoglucosan, diacids,  $\text{C}_2$  and its major precursors, the ratios of  $\text{C}_2$ /Diacids, as well as liquid water content (LWC), in-situ pH ( $\text{pH}_{\text{is}}$ ), temperature, relative humidity (RH), solar radiation, and  $\text{O}_3$  before and during the LCD in Jinan, China.

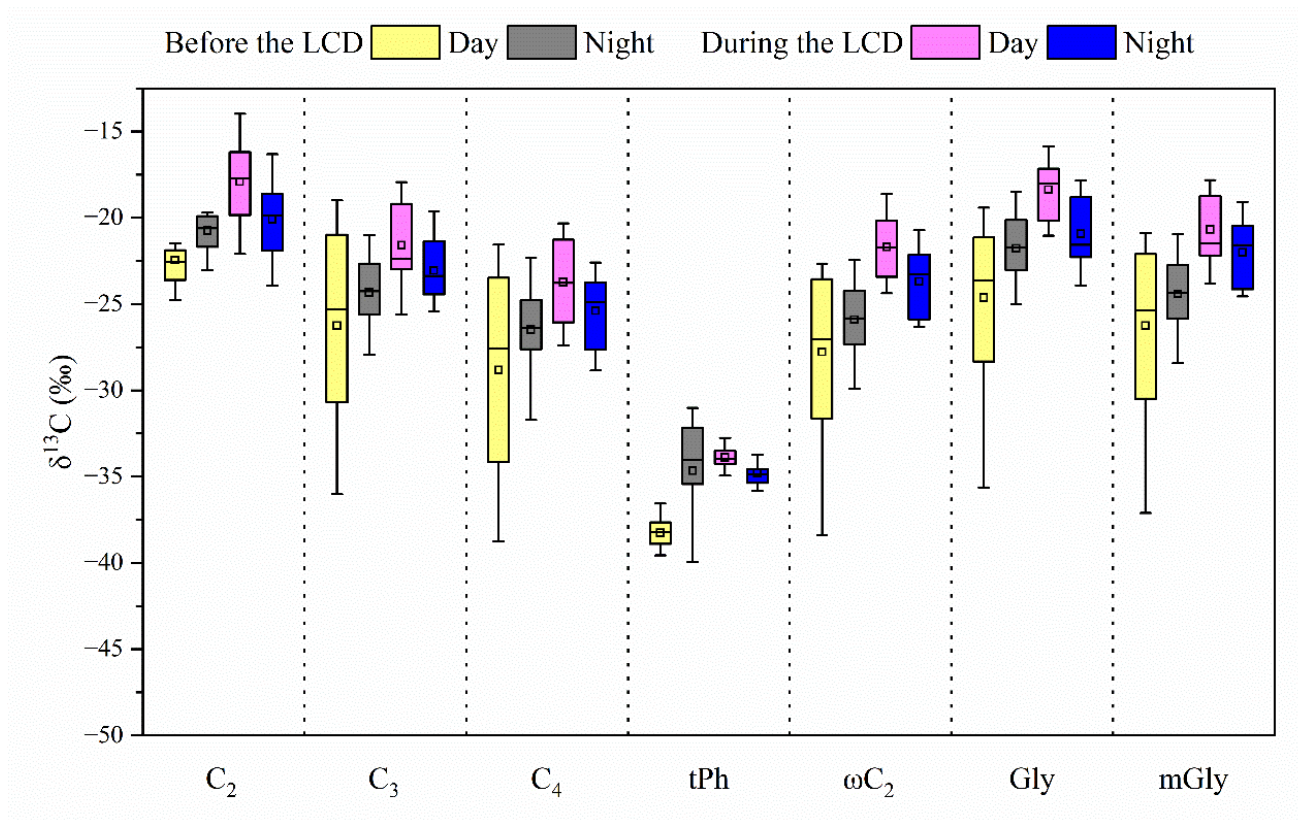


**Figure 6.** Differences in the stable carbon isotope compositions of major detected diacids ( $\text{C}_2$ – $\text{C}_4$ , tPh), the smallest oxoacids ( $\omega\text{C}_2$ ), and  $\alpha$ -dicarbonyls including Gly and mGly before and during the LCD in the atmosphere of Jinan, China.



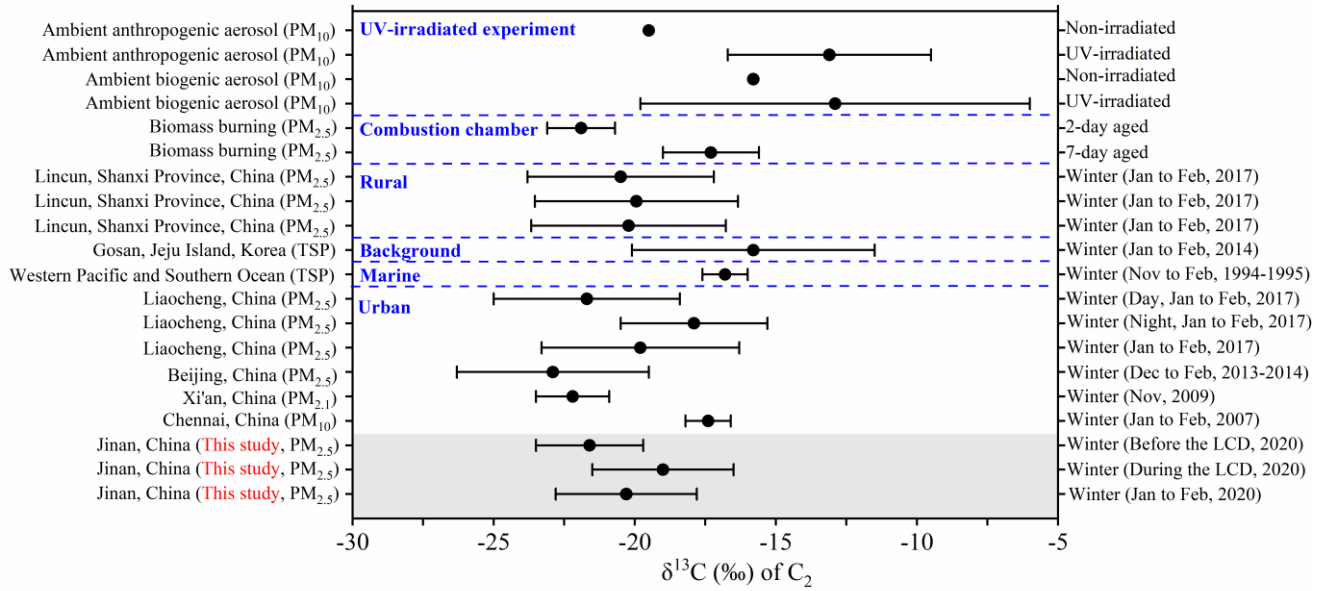
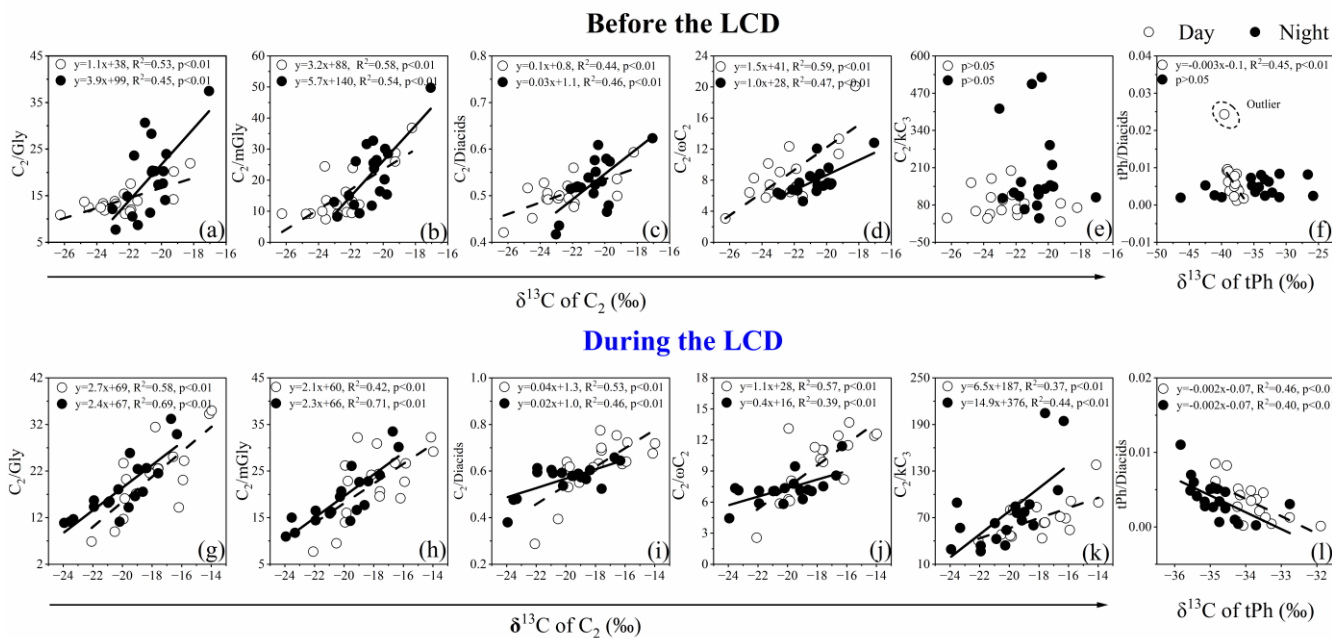


Figure 7. Comparison of stable carbon isotopic compositions ( $\delta^{13}C$ , ‰) of  $C_2$  in aerosols of Jinan with those in other regions in the winter.



965 **Figure 8.** Correlations of the  $\delta^{13}\text{C}$  of  $\text{C}_2$  with the mass ratios of  $\text{C}_2/\text{Gly}$ ,  $\text{C}_2/\text{mGly}$ ,  $\text{C}_2/\text{Diacids}$ ,  $\text{C}_2/\omega\text{C}_2$ , and  $\text{C}_2/\text{kC}_3$ , and the  $\delta^{13}\text{C}$  of tPh with the mass ratio of tPh/Diacids before and during the LCD in January to February 2020.

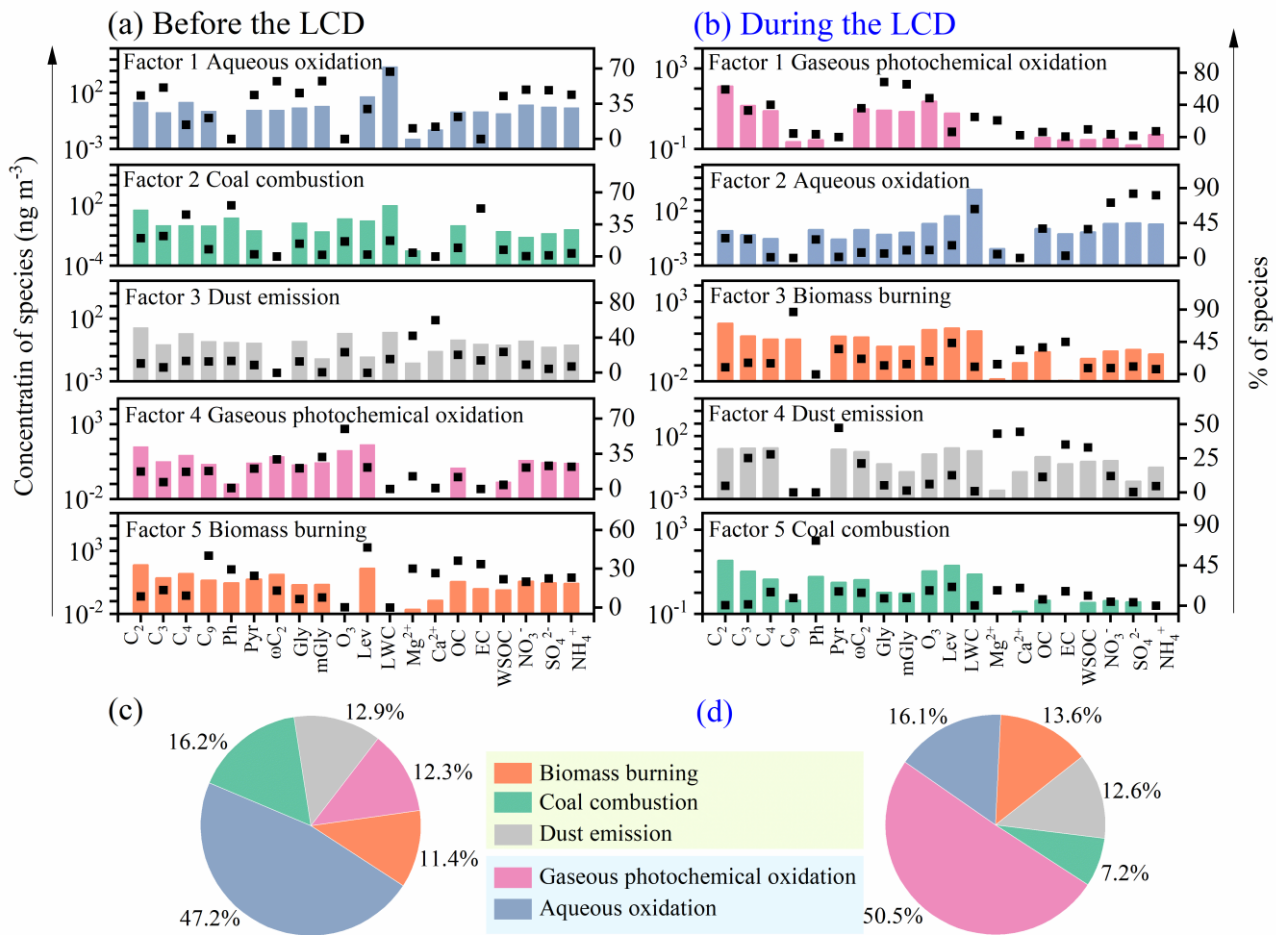


Figure 9. Source profiles of major chemical components in the PM<sub>2.5</sub> samples from Jinan (a, c) before the LCD and (b, d) during the LCD (BB: biomass burning).

970

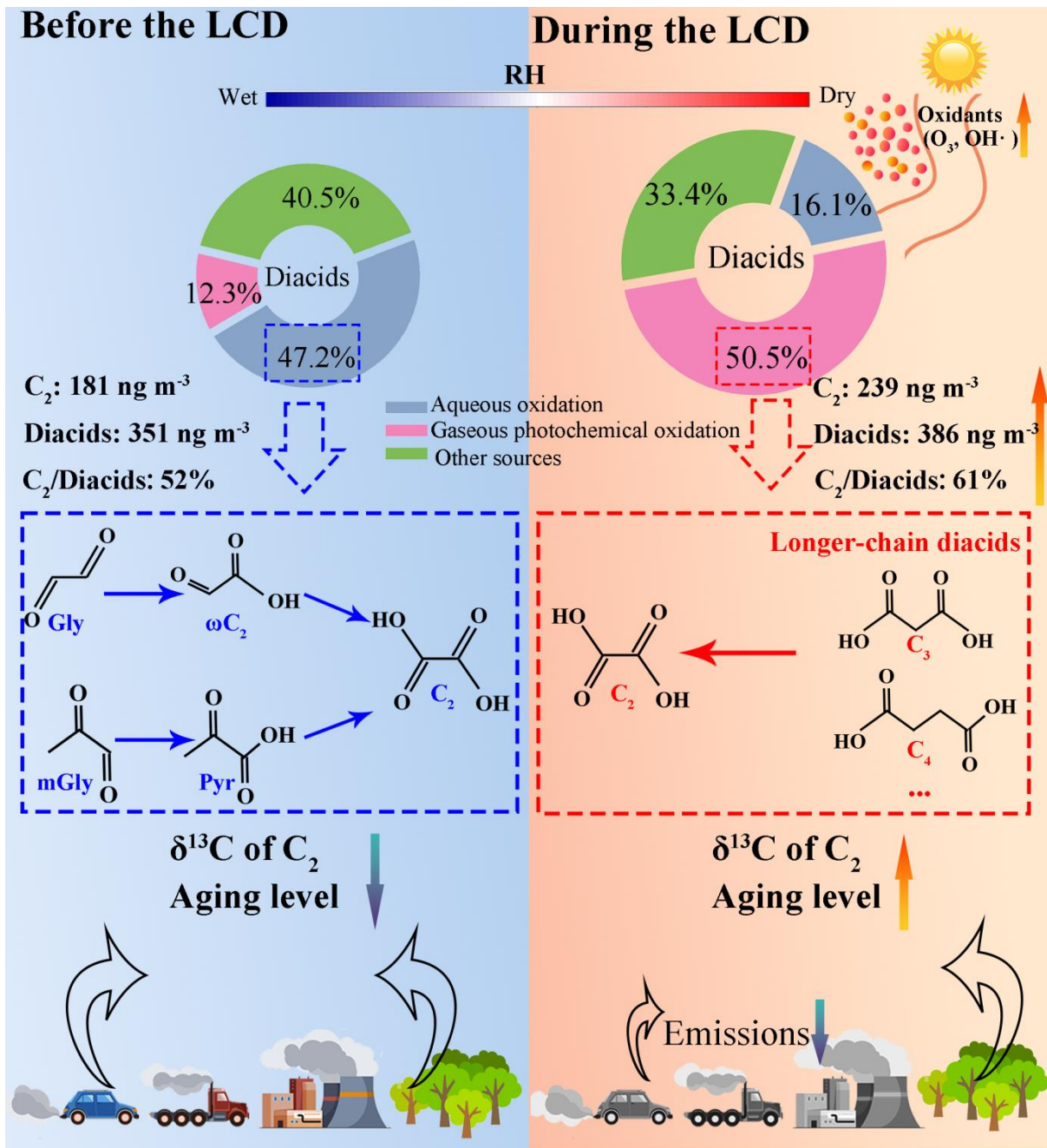


Figure 10. Schematic diagram illustrating the sources and formation mechanisms of  $C_2$  and diacids before and during the LCD.